Extensive Long-Range Entanglement at Finite Temperatures from a Nonequilibrium Bias

Shachar Fraenkel and Moshe Goldstein

Raymond and Beverly Sackler School of Physics and Astronomy, Tel Aviv University, Tel Aviv 6997801, Israel

Thermal equilibrium states of local quantum many-body systems are notorious for their spatially decaying correlations, which place severe restrictions on the types of many-body entanglement structures that may be observed at finite temperatures. These restrictions may however be defied when an out-of-equilibrium steady state is considered instead. In this paper, we study the entanglement properties of free fermions on a one-dimensional lattice that contains a generic charge- and energy-conserving noninteracting impurity, and that is connected at its edges to two reservoirs with different equilibrium energy distributions. These distributions may differ in either temperature, chemical potential, or both, thereby inducing an external bias. We analytically derive exact asymptotic expressions for several quantum information measures – the mutual information, its Rényi generalizations, and the fermionic negativity – that quantify the correlation and entanglement between two subsystems located on opposite sides of the impurity. We show that all these measures scale (to a leading order) linearly with the overlap between one subsystem and the mirror image of the other (upon reflection of the latter about the impurity), independently of the distance between the subsystems. While a simple proportionality relation between the negativity and Rényi versions of the mutual information is observed to hold at zero temperature, it breaks down at finite temperatures, suggesting that these quantities represent strong long-range correlations of different origins. Our results generalize previous findings that were limited to the case of a chemical-potential bias at zero temperature, rigorously demonstrating that the effect of long-range volume-law entanglement is robust at finite temperatures.

I. INTRODUCTION

Nonequilibrium condensed matter systems produce a rich landscape of physical phenomena, its exploration ceaselessly revealing behaviors that do not fall under the auspices of traditional equilibrium statistical mechanics. As we strive to chart the contours of this landscape, we are thus called to construct novel theoretical formalisms that could effectively capture such peculiar effects. For quantum many-body systems, a perspective that has emerged in recent years, rooted in quantum information theory, has been immensely conducive to the formulation of a theoretical language that could encompass far-from-equilibrium physics. This perspective uses measures of the amount and the spread of quantum information stored in the state of a system as probes for nonequilibrium many-body phenomena, allowing to describe these phenomena quantitatively, as well as to unify their description across different theoretical models.

As a marked example for the success of this approach, the proneness of a closed quantum system to reach local thermal equilibrium (or to avoid it) after a nonequilibrium quench has been repeatedly shown to be closely connected to the dynamics of entanglement and to the entanglement structure of energy eigenstates [1–9]. Additionally, quantum information measures can be used to distinguish integrable systems from nonintegrable ones. Following a quench, measures of the correlation between two disjoint subsystems of an integrable system will exhibit a transient peak even when the subsystems are separated by a large distance, while in a nonintegrable system the height of this peak practically vanishes already at a modest separation [7, 10–12], a clear signature of information scrambling [13–15].

These long-range quantum correlations within an integrable system can be made stationary rather than transient, if one considers an open system instead of a closed one. Several recent studies [16–20] have revealed examples of steady states of open free-fermion systems in which the mutual information (MI, a correlation measure that will be precisely defined below) between subsystems follows a volume law, meaning that it scales linearly with the size of the subsystems in question. Such scaling of the MI is exclusive to nonequilibrium systems: for two subsystems comprising a system at thermal equilibrium, their MI is known to adhere to an area law [21], meaning that it scales linearly with the size of their shared boundary (we note that at a zero-temperature ground state this area law may be violated, but only to a logarithmic order in subsystem size [22–24]; such a logarithmic violation has also been predicted for a nonequilibrium state beyond zero temperature [25, 26]).

All of these recent studies considered the steady state of a system that is subjected to an external chemical-potential bias, and that is characterized by inhomogeneity: Refs. [16, 17] considered fermions in a disordered potential, relating the scaling of the MI to the phase transition of the 3D noninteracting Anderson model; Refs. [18, 20] examined a quantum variant of the 1D symmetric simple exclusion process, where fermions experience random hopping between lattice sites; and in Ref. [19] we looked at a 1D tight-binding model hosting a noninteracting impurity, and investigated the zero-temperature correlations between subsystems on opposite sides of the impurity. Refs. [16, 19] have additionally shown that the volume-law scaling applies also to the

fermionic negativity, a genuine measure of quantum entanglement between subsystems (a precise definition is given below).

In this context, Ref. [19] is distinct in that it considered the correlation between spatially separated subsystems. We have shown there that the extensive scaling of the MI and the negativity holds even in the long-range limit, where the distance between the subsystems is much larger than their lengths, provided that their distances from the impurity are similar. This remarkable entanglement structure is generated by fermions occupying the excess energy states of the edge reservoir with the higher chemical potential, and it stems from the coherence between the reflected part and the transmitted part of each fermion that is scattered off the impurity.

The emergence of extensive long-range entanglement in the steady state of an inhomogeneous free system is close in spirit to the aforementioned transient MI peak in a post-quench homogeneous integrable system, as both phenomena arise due to the absence of decoherence in the system, and the consequent ability of particles (or quasi-particles) to carry quantum information over large distances while unobstructed. It is therefore natural to ponder to what extent the mechanism observed in the case of Ref. [19] is general, and may lead to similar entanglement structures in steady states beyond that particular case.

In this work, we make progress in this direction by studying the same free-fermion model as in Ref. [19], but considering a more general form of the external nonequilibrium bias. Instead of assuming that the edge reservoirs are at zero temperature with different chemical potentials, we relax the assumption by requiring simply that the energy distributions in the two reservoirs are different. This includes the possibility of finite-temperature reservoirs, and in particular the steady state formed due to a temperature bias with no net particle current.

We analytically derive the asymptotic forms of the MI and negativity within the steady state, and find the same volume-law scaling as the one observed in the zero-temperature case: the two quantities scale linearly with the mirror-image overlap between the two subsystems; that is, the number of overlapping lattice sites between one subsystem and the mirror-image of the other, when reflected about the location of the impurity. On our way there, we also obtain exact expressions for families of quantities that generalize the MI and negativity, which are collectively referred to as Rényi generalizations, and which contain additional information on the correlation structure of the steady state. Our results thus contribute also to the growing body of analytical work on quantum correlations in many-body systems containing impurities, both in and out of equilibrium [27–38].

The paper is structured as follows. In Sec. II we present the definitions of the quantum information measures that lie at the center of our analysis, and explain their importance in general. In Sec. III we describe the model of interest and define the subsystems for which correlation measures are to be computed. Sec. IV contains our main analytical results, as well as a discussion of their physical implications and an intuitive explanation enabling their natural interpretation. The details of the derivation of these results appear in Sec. V, which is supplemented by three technical appendices. We conclude the paper with Sec. VI, which summarizes our main messages and looks ahead at future directions of research.

II. REVIEW OF RELEVANT QUANTUM INFORMATION QUANTITIES

The following section provides a brief review of the quantum information quantities studied in this work, including their formal definitions and their meanings in terms of many-body correlations. Throughout this section, we will use the notation ρ_X to refer to the reduced density matrix of some subsystem X, which is the density matrix left following a partial trace of the system density matrix over the degrees of freedom of X^c, the complement of X.

We first define the von Neumann entropy of subsystem X as

$$S_X = -\text{Tr}[\rho_X \ln \rho_X], \tag{1}$$

and its nth Rényi entropy as

$$S_X^{(n)} = \frac{1}{1-n} \ln \text{Tr}[(\rho_X)^n]. \tag{2}$$

These quantities satisfy $\lim_{n\to 1} S_X^{(n)} = S_X$, a relation which is commonly used to extract the von Neumann entropy, as Rényi entropies tend to be more directly accessible, both in terms of analytical computation as well as in terms of experimental measurement [39–43]. When the total state of the system is pure, the von Neumann and Rényi entropies quantify the entanglement between X and X^c [44]; our current work, however, deals in general with states that are globally mixed.

The correlation between any two disjoint subsystems X_1 and X_2 can be quantified through their mutual information (MI), defined as

$$\mathcal{I} = S_{X_1} + S_{X_2} - S_{X_1 \cup X_2}. \tag{3}$$

The MI is non-negative by its definition, and serves as a measure of the total classical and quantum correlations between X_1 and X_2 [45]. In analogy to the von Neumann entropy, the MI can be expressed as the $n \to 1$ limit of the quantity

$$\mathcal{I}^{(n)} = S_{X_1}^{(n)} + S_{X_2}^{(n)} - S_{X_1 \cup X_2}^{(n)}, \tag{4}$$

to which we refer as the Rényi mutual information (RMI). The RMI vanishes when X_1 and X_2 are completely uncorrelated (i.e., when $\rho_{X_1 \cup X_2} = \rho_{X_1} \otimes \rho_{X_2}$), but is generally problematic as a measure of correlations between subsystems, as it lacks certain desirable properties: unlike the

MI, the RMI may increase under local operations (i.e., operations restricted to either X_1 or X_2), and it can also be negative [46, 47]. However, the accessibility of the Rényi entropies makes the RMI a useful tool in the extraction of the MI, and, as we will show, in our case of interest the MI and the RMI follow a similar scaling law.

There are also alternative definitions of index-dependent quantities that generalize the MI, from which the latter can be obtained through analytic continuation. One such quantity, which was recently studied in the context of quantum field theories [48], is the Petz-Rényi mutual information (PRMI):

$$\mathcal{D}^{(n)} = \frac{1}{n-1} \ln \mathrm{Tr} \left[(\rho_{X_1 \cup X_2})^n \, (\rho_{X_1} \otimes \rho_{X_2})^{1-n} \right]. \quad (5)$$

The PRMI is a positive measure of correlations which satisfies $\lim_{n \to 1} \mathcal{D}^{(n)} = \mathcal{I}$. It provides a set of bounds on the correlation function of any pair of operators in which one operator is supported on X_1 and the other is supported on X_2 [21, 48].

Given that the MI does not distinguish between classical and quantum correlations, it is desirable to study a measure that is sensitive only to the latter. Such a measure is given by the fermionic negativity [49] (inspired by the logarithmic negativity [50, 51]), defined as

$$\mathcal{E} = \ln \mathrm{Tr} \sqrt{(\widetilde{\rho}_{X_1 \cup X_2})^\dagger \, \widetilde{\rho}_{X_1 \cup X_2}}, \quad (6)$$

where the operation $\rho_{X_1 \cup X_2} \to \widetilde{\rho}_{X_1 \cup X_2}$ is the fermionic partial transpose (which is equivalent to a partial time-reversal transformation, applied to either X_1 or X_2). The negativity $\mathcal{E}$ measures the entanglement between X_1 and X_2 within any mixed state of $X_1 \cup X_2$, and is particularly useful when this state is Gaussian, as in this case its computation is significantly simplified [49, 52, 53], as we further explain in Sec. V. Again, one can introduce an index-dependent quantity, the Rényi negativity, which generically is easier to compute and measure. The Rényi negativity is defined for any even integer n as

$$\mathcal{E}^{(n)} = \ln \mathrm{Tr} \left[\left((\widetilde{\rho}_{X_1 \cup X_2})^\dagger \, \widetilde{\rho}_{X_1 \cup X_2} \right)^{n/2} \right], \quad (7)$$

and satisfies $\lim_{n \to 1} \mathcal{E}^{(n)} = \mathcal{E}$. Beyond being auxiliary quantities for the computation of the negativity, the Rényi negativities can be used to reconstruct the negativity spectrum [54, 55], i.e., the spectrum of $\widetilde{\rho}_{X_1 \cup X_2}$. However, it is not itself a proper measure of correlations between X_1 and X_2, as it may be nonzero even when these subsystems are not correlated: if the state $\rho_{X_1 \cup X_2}$ is separable, then $\mathcal{E}^{(n)} = (1-n) S_{X_1 \cup X_2}^{(n)}$, meaning that $\mathcal{E}^{(n)}$ is nonzero if $\rho_{X_1 \cup X_2}$ is also mixed.

III. THE SYSTEM AND ITS STEADY STATE

Here we define precisely the model and the nonequilibrium state that are the subject of this work, and set up the notation with which we will express our analytical results.

We consider a one-dimensional lattice, the sites of which can be occupied by free spinless fermions. The lattice is connected at its edges to two reservoirs of free fermions, both of which at equilibrium: the left reservoir is characterized by a chemical potential μ_L and a temperature T_L, and the right reservoir is characterized by a chemical potential μ_R and a temperature T_R. The lattice itself is modeled as a tight-binding chain which is homogeneous almost everywhere. The homogeneity of the chain is broken only in a small region near its center, a region which constitutes a noninteracting impurity that conserves the number of particles. The model is therefore governed by a Hamiltonian of the form

$$\mathcal{H} = -\eta \sum_{m=m_0}^{\infty} \left[c_m^\dagger c_{m+1} + c_{-m}^\dagger c_{-m-1} + \mathrm{h.c.} \right] + \mathcal{H}_{\mathrm{scat}}, \quad (8)$$

with $\eta > 0$ being a real hopping amplitude, c_m being the fermionic annihilation operator associated with the site m, m_0 being some fixed integer, and $\mathcal{H}_{\mathrm{scat}}$ being the term associated with the impurity. $\mathcal{H}_{\mathrm{scat}}$ is a combination of quadratic terms of the form $c_m^\dagger c_{m'}$, with the indices m, m' being limited to the region $-m_0 \leq m, m' \leq m_0$, or possibly associated with additional sites attached to this region from the side. Realistically, the lattice must be finite considering its attachment to edge reservoirs, but the infinite sum appearing in Eq. (8) is still a valid representation if we interpret the correlation structure that we discover as pertaining to a region around the impurity that is much smaller than the actual length of the lattice.

The single-particle energy eigenbasis of the Hamiltonian in Eq. (8) is generically comprised of bound states, that are exponentially localized at the impurity, and of extended states [56]. The effect of the bound states is negligible when considering correlations between subsystems that exclude the impurity, as we do in this work, and we therefore ignore those states. The form of the extended states, on the other hand, is what gives rise to the unusual entanglement structure that we find here. Outside the impurity region, this form can be concisely represented by a unitary scattering matrix $S(k)$ of size 2×2 [57], defined for any $0 < k < \pi$:

$$S(k) = \begin{pmatrix} r_L(k) & t_R(k) \\ t_L(k) & r_R(k) \end{pmatrix}. \quad (9)$$

The diagonal entries of $S(k)$ are reflection amplitudes, and its off-diagonal entries are transmission amplitudes. We let $\mathcal{R} = |r_L|^2 = |r_R|^2$ and $\mathcal{T} = |t_L|^2 = |t_R|^2$ denote the reflection and transmission probabilities, respectively. Since $S(k)$ is unitary, $\mathcal{T}(k) + \mathcal{R}(k) = 1$.

The extended states $|k\rangle$ are parameterized by the momentum coordinate k with $0 < |k| < \pi$, and are associated with the single-particle energy spectrum $\epsilon(k) = -2\eta \cos k$. They are comprised of left scattering states, defined for any $0 < k < \pi$ by the wavefunction
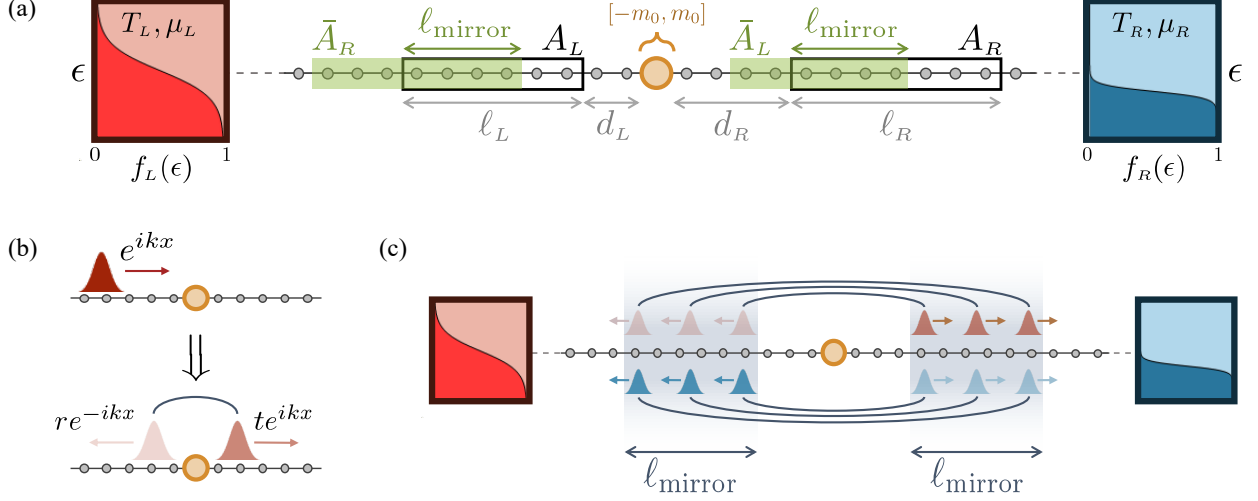
Figure 1. (a) A schematic illustration of the model, with an exemplary choice of subsystems. A long one-dimensional chain of lattice sites is homogeneous almost everywhere, apart from a small middle region (represented by the larger circle) which constitutes a noninteracting impurity, and spans the sites with indices $-m_0 \leq m \leq m_0$. At its distant edges, the system is attached to two free-fermion reservoirs with temperatures T_i and chemical potentials μ_i ($i = L,R$), giving rise to Fermi-Dirac energy distributions $f_i(\epsilon)$ (Eq. (12)). The subsystems A_L and A_R, on opposite sides of the impurity, are marked by black empty rectangles, with the length and distance from the impurity of A_i denoted by ℓ_i and d_i, respectively. $\bar{A}_i = \{m| -m \in A_i\}$ are the mirror images of the subsystems with respect to the middle of the chain, and ℓ_{mirror} (defined in Eq. (15)) is the length of the overlap between one subsystem and the mirror image of the other. (b) The homogeneity-breaking impurity induces the scattering of an incoming wavepacket, concentrated around a certain energy. This creates a transmitted part and a reflected part with (generally energy-dependent) amplitudes t and r (respectively), such that the two parts are coherently correlated. (c) At each energy where, as a result of the nonequilibrium bias, there is an excess of particles coming from one of the edge reservoirs, entanglement between mirroring regions in the chain is generated due to the coherent correlation between the counter-propagating scattered parts. The number of wavepackets shared by the mirroring regions is proportional to their length, leading to volume-law entanglement.

$$\langle m|k\rangle = \begin{cases} e^{ikm} + r_L(|k|)\,e^{-ikm} & m < -m_0, \\ t_L(|k|)\,e^{ikm} & m > m_0, \end{cases} \quad (10)$$

together with right scattering states, given for any $-\pi < k < 0$ by

$$\langle m|k\rangle = \begin{cases} t_R(|k|)\,e^{ikm} & m < -m_0, \\ e^{ikm} + r_R(|k|)\,e^{-ikm} & m > m_0. \end{cases} \quad (11)$$

The form of the wavefunctions inside the impurity region is irrelevant when considering correlations between subsystems that exclude this region. Their form outside the impurity region clearly depends only on the scattering matrix in Eq. (9).

The many-body nonequilibrium steady state of the system is determined by the single-particle energy distributions of the two edge reservoirs. In each reservoir, a state with energy ϵ is occupied with the probability $f_i(\epsilon)$ (with $i = L,R$), which is given by the equilibrium Fermi-Dirac distribution:

$$f_i(\epsilon) = \frac{1}{\exp\left[(\epsilon - \mu_i)/T_i\right] + 1}. \quad (12)$$

In what follows, we will express these distributions as functions of k, i.e., $f_i(k) = f_i(\epsilon(k))$. Within the lattice, an energy eigenstate $|k\rangle$ is therefore occupied according to the distribution $\widetilde{f}(k)$, defined as

$$\widetilde{f}(k) = \begin{cases} f_R(k) & k < 0, \\ f_L(k) & k > 0. \end{cases} \quad (13)$$

In other words, if we let c_k denote the annihilation operator associated with the single-particle state $|k\rangle$, the nonequilibrium steady state ρ_{NESS} of the system is given by

$$\rho_{\mathrm{NESS}} = \prod_k \left[\widetilde{f}(k)\, c_k^\dagger c_k + \left(1 - \widetilde{f}(k)\right) c_k c_k^\dagger \right], \quad (14)$$

which is a Gaussian state.

Throughout the rest of the paper, we address the correlations between two subsystems, denoted by A_L and A_R, as measured by the different quantities reviewed in Sec. II. The interval A_L is located to the left of the impurity and spans the sites m with $-d_L - \ell_L \leq m + m_0 \leq -d_L - 1$, while the interval A_R is located

to the right of the impurity and spans the sites m with $d_R + 1 \leq m - m_0 \leq d_R + \ell_R$. Thus, ℓ_i denotes the number of sites in A_i, and d_i represents the number of sites separating the impurity region from the nearest boundary of A_i ($i = L,R$). The length scales ℓ_i and d_i are assumed to be much larger than $2m_0 + 1$, which is the size of the impurity.

As will become apparent when discussing our results, it is also useful to introduce notations for the mirror images of these subsystems: we let $\bar{A}_i = \{m| - m \in A_i\}$ denote the set of sites obtained by reflecting the sites in A_i about the middle site $m = 0$, which also marks the center of the impurity. We can then refer to either $\bar{A}_L \cap A_R$ or $A_L \cap \bar{A}_R$ as the mirror-image overlap between the two subsystems, i.e., the overlap between one subsystem and the mirror image of the other. Finally, we let $\ell_{\text{mirror}} = \left|\bar{A}_L \cap A_R\right| = \left|A_L \cap \bar{A}_R\right|$ denote the length of this overlap, which is equivalent to defining

$$\ell_{\text{mirror}} = \max\{\min\{d_L + \ell_L, d_R + \ell_R\} - \max\{d_L, d_R\}, 0\}. \tag{15}$$

The length scale ℓ_{mirror} is the one with respect to which the correlation measures that we consider exhibit their volume-law scaling. Importantly, it depends on the distances d_L and d_R of the subsystems from the impurity only through $d_L - d_R$.

A schematic illustration of the system appears in Fig. 1(a), where we also show an example for a choice of A_L and A_R, and indicate the associated length scales.

IV. EXACT RESULTS

In this section we present the main results of our work, which are the exact formulae for the leading-order asymptotics of the correlation measures defined in Sec. II, when applied to the model and subsystems defined in Sec. III. We discuss the interpretation of these analytical formulae and their various limits, and compare them to numerical results. The derivation of the analytical results is detailed in Sec. V.

Our analysis shows that the nth RMI between A_L and A_R scales as

$$\begin{aligned}
\mathcal{I}^{(n)} \sim \frac{\ell_{\text{mirror}}}{1-n} \int_0^\pi \frac{dk}{2\pi} &\Big\{\ln[(\mathcal{T}f_L + \mathcal{R}f_R)^n + (1 - \mathcal{T}f_L - \mathcal{R}f_R)^n] \\
&+ \ln[(\mathcal{R}f_L + \mathcal{T}f_R)^n + (1 - \mathcal{R}f_L - \mathcal{T}f_R)^n] \\
&- \ln[(f_L)^n + (1-f_L)^n] - \ln[(f_R)^n + (1-f_R)^n]\Big\},
\end{aligned} \tag{16}$$

while the PRMI is given by

$$\begin{aligned}
\mathcal{D}^{(n)} \sim \frac{\ell_{\text{mirror}}}{n-1} \int_0^\pi \frac{dk}{2\pi} \ln\Bigg[&\mathcal{T}\left(\frac{(f_L)^n}{(\mathcal{T}f_L + \mathcal{R}f_R)^{n-1}} + \frac{(1-f_L)^n}{(1 - \mathcal{T}f_L - \mathcal{R}f_R)^{n-1}}\right)\left(\frac{(f_R)^n}{(\mathcal{R}f_L + \mathcal{T}f_R)^{n-1}} + \frac{(1-f_R)^n}{(1 - \mathcal{R}f_L - \mathcal{T}f_R)^{n-1}}\right) \\
&+ \mathcal{R}\left(\frac{(f_L)^n}{(\mathcal{R}f_L + \mathcal{T}f_R)^{n-1}} + \frac{(1-f_L)^n}{(1 - \mathcal{R}f_L - \mathcal{T}f_R)^{n-1}}\right)\left(\frac{(f_R)^n}{(\mathcal{T}f_L + \mathcal{R}f_R)^{n-1}} + \frac{(1-f_R)^n}{(1 - \mathcal{T}f_L - \mathcal{R}f_R)^{n-1}}\right)\Bigg].
\end{aligned} \tag{17}$$

By taking the limit $n \to 1$ of either Eq. (16) or Eq. (17), we obtain the MI, which reads

$$\begin{aligned}
\mathcal{I} \sim \ell_{\text{mirror}} \int_0^\pi \frac{dk}{2\pi} \Big\{ &-(\mathcal{T}f_L + \mathcal{R}f_R)\ln(\mathcal{T}f_L + \mathcal{R}f_R) - (1 - \mathcal{T}f_L - \mathcal{R}f_R)\ln(1 - \mathcal{T}f_L - \mathcal{R}f_R) + f_L \ln f_L + (1-f_L)\ln(1-f_L) \\
&-(\mathcal{R}f_L + \mathcal{T}f_R)\ln(\mathcal{R}f_L + \mathcal{T}f_R) - (1 - \mathcal{R}f_L - \mathcal{T}f_R)\ln(1 - \mathcal{R}f_L - \mathcal{T}f_R) + f_R \ln f_R + (1-f_R)\ln(1-f_R)\Big\}.
\end{aligned} \tag{18}$$

Furthermore, the fermionic negativity between the two subsystems is found to scale as

$$\begin{aligned}
\mathcal{E} \sim \ell_{\text{mirror}} \int_0^\pi \frac{dk}{2\pi} \ln\Big[&f_L + f_R - 2f_L f_R \\
&+ \sqrt{[1 - f_L - f_R + 2f_L f_R]^2 + 4\mathcal{T}\mathcal{R}(f_L - f_R)^2}\Big]. \tag{19}
\end{aligned}$$

Thus, the measures in Eqs. (16)–(19) all scale linearly

with ℓ_{mirror}, signaling volume-law long-range correlation and entanglement between the two subsystems (recall that ℓ_{mirror} depends only on $d_L - d_R$, hence the use of the term "long-range").

We may immediately observe another property that these measures all share: their volume-law terms vanish if, for all momenta $k \in [0, \pi]$, either $f_L(k) = f_R(k)$ or $\mathcal{T}(k) \in \{0, 1\}$. The first condition corresponds to the absence of a nonequilibrium bias at the energy $\epsilon(k)$, while the second translates into the impurity being triv-
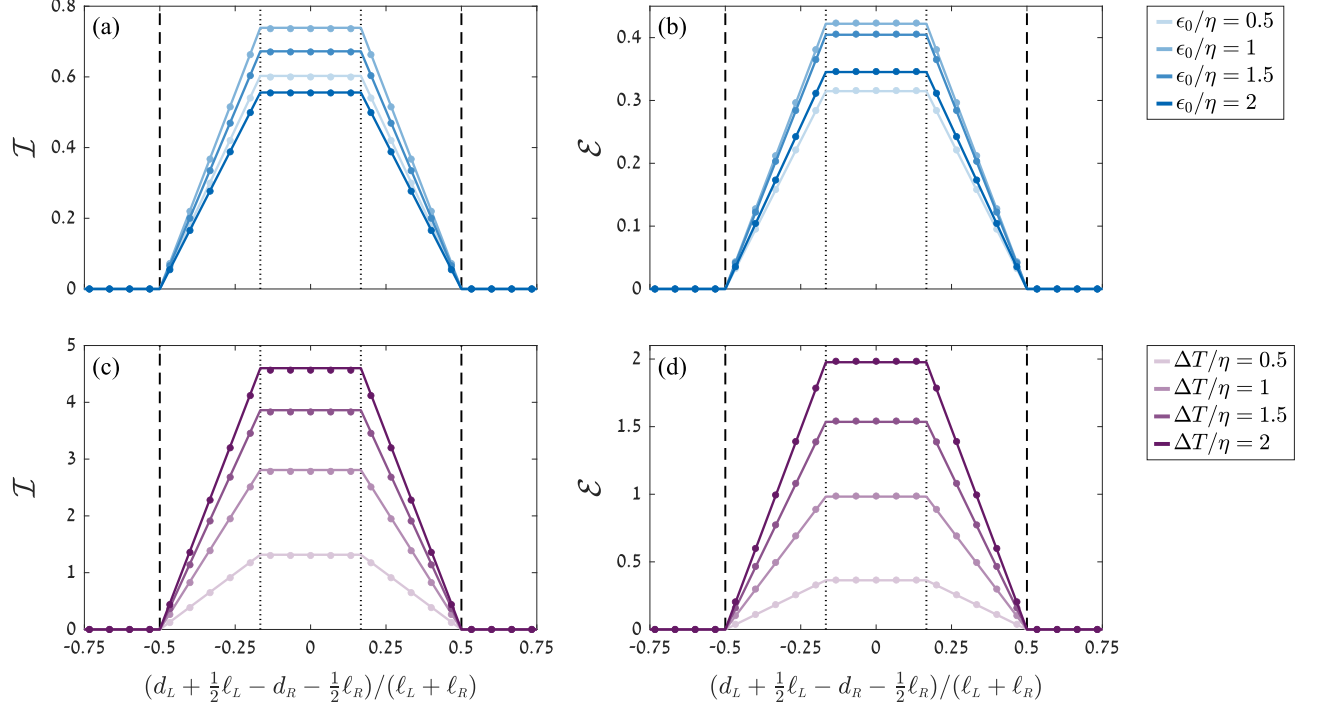
Figure 2. The mutual information and negativity between A_L and A_R in the resonant level model, under a temperature bias and with no chemical-potential bias, setting $\mu_L = \mu_R = 0$. In all panels, the subsystem lengths are fixed to be $\ell_L = 100$ and $\ell_R = 200$, while their relative distance from the impurity $d_L - d_R$ is varied. Note that $d_i + \frac{1}{2}\ell_i$, appearing in the label of the horizontal axis, is the distance from the midpoint of A_i to the impurity ($i = L,R$). Continuous lines represent analytical results (computed from Eqs. (18) and (19) for the MI and negativity, respectively), while dots represent numerical results (computed in the limit $d_i/\ell_i \to \infty$, as explained in Subsec. V A 2). In each panel, between the two vertical dotted lines the values of $d_L - d_R$ are such that $\bar{A}_L \subset A_R$ (i.e., maximal mirror-image overlap), and between the two vertical dashed lines they are such that $\bar{A}_L \cap A_R \neq \phi$ (i.e., nonzero mirror-image overlap). Top panels: (a) The MI and (b) the negativity for different values of the impurity on-site energy ϵ_0, with $T_L = 2\eta$ and $T_R = \eta$. Bottom panels: (c) The MI and (d) the negativity for different values of the temperature bias $\Delta T = T_L - T_R$, with $T_R = 0.5\eta$ and $\epsilon_0 = \eta$.

ial, meaning perfectly transmissive or perfectly reflective, at that energy. In contrast, if these conditions fail to apply (for a nonzero-measure subset of $[0,k]$) – i.e., in the presence of both a nonequilibrium bias and nontrivial scattering – then the volume-law terms in Eqs. (16)–(19) are all positive. The bias and the nontrivial scattering by the impurity are therefore necessary and sufficient conditions for the emergence of the observed strong long-range entanglement in the steady state.

These two conditions together also render the functions $\mathcal{T}f_L + \mathcal{R}f_R$ and $\mathcal{R}f_L + \mathcal{T}f_R$ incompatible with equilibrium distributions; that is, none of them can be written using an effective temperature and an effective chemical potential. These two functions are featured in Eqs. (16)–(18) as the arguments of entropic functions (e.g., $-x\ln x - (1-x)\ln(1-x)$ in Eq. (18)) that otherwise tend to arise when calculating entropic measures for some equilibrium state, with the appropriate equilibrium distribution as their argument. The nonequilibrium nature of the steady-state correlations is thus made conspicuous by the mathematical structure of Eqs. (16)–(18).

As in the zero-temperature case, the origin of the volume-law long-range correlations can be interpreted by considering that, at each energy participating in the nonequilibrium bias, there is an excess of particles incoming from one reservoir rather than the other. A wavepacket representing each such particle splits at the impurity into a coherent superposition of two counter-propagating wavepackets, with the superposition amplitudes determined by the scattering matrix (illustrated in Fig. 1(b)). With the two wavepackets moving uninterruptedly with group velocities of the same magnitude, they generate entanglement between faraway sites that have an equal distance from the impurity. This effect would have been canceled within the many-body state if the same current of particles at that energy had flowed in the opposite direction, yet the nonequilibrium bias ensures that this is not so. Given the stationary rate of incoming particles, mirroring regions share such correlated wavepackets in a manner proportional to their length (illustrated in Fig. 1(c)). The only difference between this interpretation and the more specific picture of the zero-
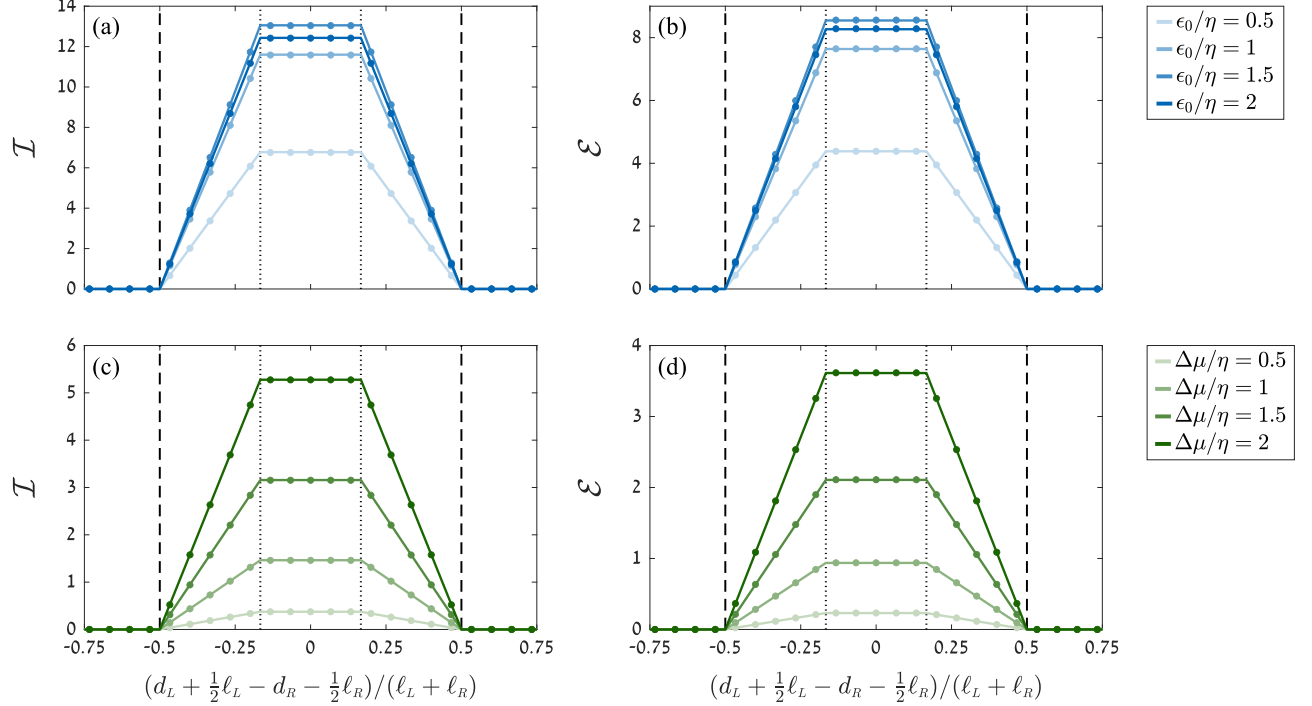
Figure 3. The mutual information and negativity between A_L and A_R in the resonant level model, under a chemical-potential bias and with no temperature bias, setting $T_L = T_R = \eta$. In all panels, the subsystem lengths are fixed to be $\ell_L = 100$ and $\ell_R = 200$, while their relative distance from the impurity $d_L - d_R$ is varied. Note that $d_i + \frac{1}{2}\ell_i$, appearing in the label of the horizontal axis, is the distance from the midpoint of A_i to the impurity ($i = L, R$). Continuous lines represent analytical results (computed from Eqs. (18) and (19) for the MI and negativity, respectively), while dots represent numerical results (computed in the limit $d_i/\ell_i \to \infty$, as explained in Subsec. V A 2). In each panel, between the two vertical dotted lines the values of $d_L - d_R$ are such that $\bar{A}_L \subset A_R$ (i.e., maximal mirror-image overlap), and between the two vertical dashed lines they are such that $\bar{A}_L \cap A_R \neq \phi$ (i.e., nonzero mirror-image overlap). Top panels: (a) The MI and (b) the negativity for different values of the impurity on-site energy ϵ_0, with $\mu_L = -\mu_R = 1.5\eta$. Bottom panels: (c) The MI and (d) the negativity for different values of the chemical-potential bias $\Delta\mu = \mu_L - \mu_R$, with $\mu_R = 0$ and $\epsilon_0 = \eta$.

temperature case is simply that, in the latter, there is a certain window of energies in which particles emerge only from one of the reservoirs, while in the former particles possibly emerge from both reservoirs and still generate entanglement due to an occupation bias.

There is, however, a noteworthy quantitative difference in the results between the zero-temperature case and the more general scenario. By plugging $T_L = T_R = 0$ into Eqs. (16) and (19), we recover the results that were reported in Ref. [19] for the RMI and the negativity. That is, letting $k_+ = \max\{k_{F,L}, k_{F,R}\}$ and $k_- = \min\{k_{F,L}, k_{F,R}\}$ denote the Fermi momenta of the two reservoirs (with $k_{F,i} = \epsilon^{-1}(\mu_i)$), we obtain

$$\mathcal{I}^{(n)} \sim \frac{\ell_{\mathrm{mirror}}}{1-n} \int_{k_-}^{k_+} \frac{dk}{\pi} \ln[\mathcal{T}^n + \mathcal{R}^n] \,, \tag{20}$$

and find that the negativity and the $n = 1/2$ RMI satisfy (to the leading order) the simple relation $\mathcal{E} \sim \frac{1}{2}\mathcal{I}^{(1/2)}$. This relation is observed in (interacting or noninteracting) integrable systems following zero-temperature

quenches, which are described by the quasi-particle picture [11], and in the post-quench early-time dynamics of local systems in general [58]. The relation $\mathcal{E} \sim \frac{1}{2}\mathcal{I}^{(1/2)}$ would have stemmed trivially from the definitions of the two quantities had $A_L \cup A_R$ been in a pure state, but is otherwise nontrivial [59]. It may be interpreted as indicating that the correlations between the two subsystems are, to the leading order, purely quantum [58].

In contrast, as can be seen from a direct examination of Eqs. (16) and (19), this relation between the negativity and the $\frac{1}{2}$-RMI breaks down if at least one of the reservoirs is at a finite temperature. A similar breakdown of this relation was observed in nonequilibrium scenarios involving dissipation [60, 61], as well as in a steady state ensuing from a finite-temperature quench [26]. In a similar vein, at zero temperature we find that the result for the PRMI in Eq. (17) is simply reduced to $\mathcal{D}^{(n)} \sim \mathcal{I}^{(3-2n)}$, also implying that $\mathcal{E} \sim \frac{1}{2}\mathcal{D}^{(5/4)}$; again, such relations would have been satisfied trivially had the state of $A_L \cup A_R$ been pure [48]. This simple proportionality relation of the PRMI to either the RMI or the
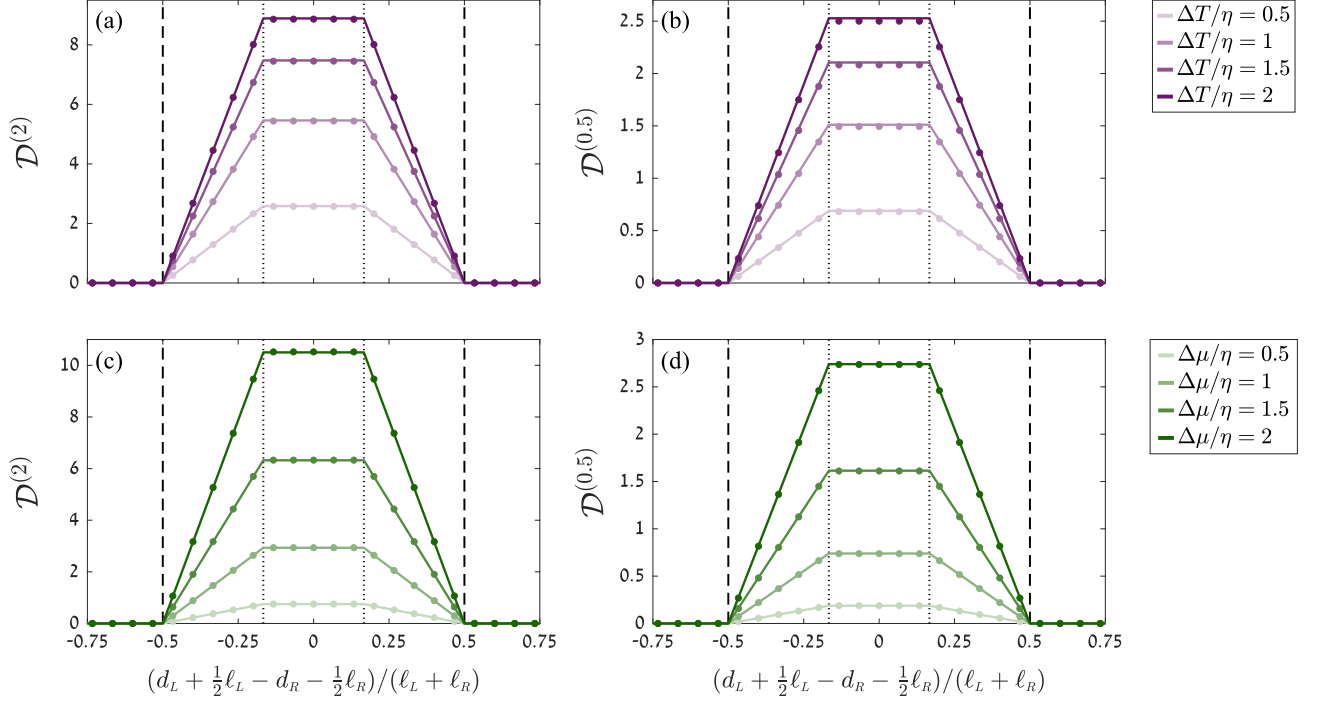
Figure 4. The Petz-Rényi mutual information between A_L and A_R in the resonant level model, setting $\epsilon_0 = \eta$. In all panels, the subsystem lengths are fixed to be $\ell_L = 100$ and $\ell_R = 200$, while their relative distance from the impurity $d_L - d_R$ is varied. Note that $d_i + \frac{1}{2}\ell_i$, appearing in the label of the horizontal axis, is the distance from the midpoint of A_i to the impurity ($i = L, R$). Continuous lines represent analytical results (computed from Eq. (17)), while dots represent numerical results (computed in the limit $d_i/\ell_i \to \infty$, as explained in Subsec. V A 2). In each panel, between the two vertical dotted lines the values of $d_L - d_R$ are such that $\bar{A}_L \subset A_R$ (i.e., maximal mirror-image overlap), and between the two vertical dashed lines they are such that $\bar{A}_L \cap A_R \neq \phi$ (i.e., nonzero mirror-image overlap). Top panels: The PRMI $\mathcal{D}^{(n)}$ for (a) $n = 2$ and (b) $n = 0.5$ in the case of a temperature bias and with no chemical-potential bias. Results are plotted for different values of the temperature bias $\Delta T = T_L - T_R$, with $T_R = 0.5\eta$ and $\mu_L = \mu_R = 0$. Bottom panels: The PRMI $\mathcal{D}^{(n)}$ for (c) $n = 2$ and (d) $n = 0.5$ in the case of a chemical-potential bias and with no temperature bias. Results are plotted for different values of the chemical-potential bias $\Delta\mu = \mu_L - \mu_R$, with $\mu_R = 0$ and $T_L = T_R = \eta$.

negativity again breaks down at finite temperatures.

To illustrate our results, in Figs. 2–3 we plot the analytical expressions for the MI and negativity (Eqs. (18) and (19), respectively) for a specific choice of an impurity model. We focus on a resonant level model, substituting $m_0 = 0$ and $\mathcal{H}_{\text{scat}} = \epsilon_0 c_0^\dagger c_0$ into Eq. (8), such that only the middle site of the chain constitutes the impurity. It is straightforward to check that in this case the momentum-dependent transmission probability is given by

$$\mathcal{T}(k) = \frac{\sin^2 k}{\sin^2 k + (\epsilon_0/2\eta)^2}. \tag{21}$$

As a corroboration of our analytical calculation, we also plot numerical results for the MI and negativity. These are computed in the long-range limit $d_i/\ell_i \to \infty$ with $d_L - d_R$ kept fixed (a limit by which the analytical expressions are unaffected), via an exact diagonalization of the two-point correlation matrix restricted to $A_L \cup A_R$, as we further elaborate in Subsec. V A 2.

Fig. 2 shows the results for a pure temperature bias, where we plot the MI and negativity for a fixed bias and different values of the impurity on-site energy ϵ_0, and vice versa. In Fig. 3 we present a similar analysis, only with a pure chemical-potential bias at a finite temperature instead of a temperature bias. In both figures, we fix the subsystem lengths ℓ_L and ℓ_R and vary $d_L - d_R$, going between no mirror-image overlap and maximal mirror-image overlap. We find an excellent agreement between the numerical results and the analytical leading-order asymptotics.

In both figures, one may easily observe that a larger nonequilibrium bias typically leads to stronger correlations, which is indeed natural considering our interpretation of the results. The dependence on the impurity on-site energy ϵ_0 is more intricate, since a change in ϵ_0 affects the transmission probability across the entire energy spectrum. Interestingly, by examining the top panels of Fig. 2, one sees that it is possible to find two values of ϵ_0 such that the MI obtained for one is larger than

the MI obtained for the other, while the negativity in the former case is smaller than in the latter. Such "non-monotonicity" between the MI and the negativity is a finite temperature effect, given that at zero temperature it is forbidden due to the simple relation between the negativity and the $\frac{1}{2}$-RMI. It is therefore a manifestation of the MI capturing strong long-range correlations beyond the quantum coherent correlations captured by the negativity.

Finally, we note that the derivation of the analytical formula for the PRMI, given in Eq. (17), relies on a recent conjecture [62] relating to the asymptotics of a certain class of determinants (see details in Subsec. V D). This fact calls for a verification of Eq. (17), by comparing it to an independent numerical computation. In Fig. 4 we plot $\mathcal{D}^{(n)}$ for two values of n and for various instances of a nonequilibrium bias, finding in all cases that Eq. (17) agrees nicely with the numerical result.

V. ANALYTICAL DERIVATION

The following section describes the derivation of the results appearing in Sec. IV. In Subsec. V A we recall general useful expressions for quantum information measures in terms of two-point correlation functions, that apply when the many-body state is Gaussian. Regarding the correlation function between sites in $A_L \cup A_R$ for our state of interest, we also recall its limit when the two subsystems are distant (originally derived in Ref. [19]), and explain the importance of this limit within our calculations. Subsequently, in Subsec. V B we derive the forms of the Rényi entropies composing (via Eq. (4)) the RMI, leading to Eq. (16); in Subsec. V C we derive the form of the negativity, given in Eq. (19); and in Subsec. V D we derive the form of the PRMI, reported in Eq. (17).

A. Reduction to two-point correlations

The analysis we present in this paper relies on the fact that, for any fermionic Gaussian many-body state (such as the one studied here), subsystem entropies and negativities are fully determined by the spectrum of two-point correlation matrices restricted to the subsystems of interest. This amounts to an exponential reduction of the numerical computational cost, and in many cases also allows to derive analytical expressions through the use of asymptotic techniques related to the structure of these correlation matrices.

For the steady state defined in (14), the two-point correlation function between any two sites can be written as

$$\left\langle c_j^\dagger c_m \right\rangle = \int_{-\pi}^{\pi} \frac{dk}{2\pi} \widetilde{f}(k) \left\langle k|j \right\rangle \left\langle m|k \right\rangle . \qquad (22)$$

A similar expression for the two-point correlation matrix applies to any Gaussian state, upon determining the appropriate single-particle states $|k\rangle$ that diagonalize the density matrix and their corresponding occupation factors $\widetilde{f}(k)$.

1. General relations for fermionic Gaussian states

Let C_X denote the two-point correlation matrix restricted to a subsystem X, meaning that its entries are given by $\left\langle c_j^\dagger c_m \right\rangle$ with $j, m \in X$. The Rényi entropies of subsystem X satisfy [63]

$$S_X^{(n)} = \frac{1}{1-n} \text{Tr} \ln[(C_X)^n + (\mathbb{I} - C_X)^n] . \qquad (23)$$

For the purpose of calculating Rényi entropies analytically, we use the relation in Eq. (23) in two different ways. First, we may expand the logarithm in the form of a power series, yielding

$$S_X^{(n)} = \frac{1}{1-n} \sum_{s=1}^{\infty} \frac{(-1)^{s+1}}{s} \text{Tr} \big[\{ (C_X)^n + (\mathbb{I} - C_X)^n - \mathbb{I} \}^s \big] . \qquad (24)$$

This expression implies that it suffices to produce a general formula for the moments of the correlation matrix, i.e., to derive the asymptotics of

$$\text{Tr}[(C_X)^p] = \int_{[-\pi,\pi]^p} \frac{d^p k}{(2\pi)^p} \prod_{j=1}^{p} \widetilde{f}(k_j) \left[\sum_{m \in X} \langle m|k_{j-1}\rangle \langle k_j|m\rangle \right] , \qquad (25)$$

for any positive integer p (we identify $k_0 = k_p$). In our case of interest, this indeed can be done in principle through the stationary phase approximation (SPA) [64], on which we elaborate in Subsec. V B.

The second way in which we may use Eq. (23) is through the root decomposition of the polynomial $z^n + (1-z)^n$, which leads to the following expression:

$$S_X^{(n)} = \frac{1}{1-n} \sum_{\gamma=-\frac{n-1}{2}}^{\frac{n-1}{2}} \ln \det \left[\mathbb{I} + \left(e^{2\pi i\gamma/n} - 1 \right) C_X \right] . \qquad (26)$$

Then, the asymptotic analysis of the entropies can be carried out if one has access to the asymptotics of the determinants in Eq. (26), which is in fact true if C_X has a Toeplitz (or block-Toeplitz) structure, since in such a case the Szegö-Widom asymptotic formula can be employed [65]. As we explain below, this required structure arises in our computation even when the restricted correlation matrices of the subsystems of interest do not possess it themselves.

The treatment of Rényi negativities is closely analogous to that of Rényi entropies. For a fermionic Gaussian state, negativities between two subsystems X_1 and

X_2 can be expressed using $C_{X_1 \cup X_2}$ and a transformed two-point correlation matrix given by

$$C_\Xi = \frac{1}{2}\left[\mathbb{I} - (\mathbb{I} + \Gamma_+ \Gamma_-)^{-1}(\Gamma_+ + \Gamma_-)\right], \qquad (27)$$

where we defined the covariance matrices

$$\Gamma_\pm = \begin{pmatrix} \pm i\mathbb{I}_{|X_1|} & 0 \\ 0 & \mathbb{I}_{|X_2|} \end{pmatrix}(\mathbb{I} - 2C_{X_1 \cup X_2})\begin{pmatrix} \pm i\mathbb{I}_{|X_1|} & 0 \\ 0 & \mathbb{I}_{|X_2|} \end{pmatrix}, \qquad (28)$$

assuming that the first $|X_1|$ indices designating the entries of $C_{X_1 \cup X_2}$ correspond to the sites of subsystem X_1. Using the matrix defined in Eq. (27), Rényi negativities can be written as [49, 52, 53]

$$\mathcal{E}^{(n)} = \mathrm{Tr}\ln\left[(C_\Xi)^{n/2} + (\mathbb{I} - C_\Xi)^{n/2}\right] \\ + \frac{n}{2}\mathrm{Tr}\ln\left[(C_{X_1 \cup X_2})^2 + (\mathbb{I} - C_{X_1 \cup X_2})^2\right]. \qquad (29)$$

Additionally, in Ref. [19] we showed that an equivalent

way of writing this equality is

$$\mathcal{E}^{(n)} = \mathrm{Tr}\ln\left[\prod_{\gamma = -\frac{n-1}{2}}^{\frac{n-1}{2}}(\mathbb{I} - C_\gamma)\right], \qquad (30)$$

where we introduced for $\gamma = -\frac{n-1}{2}, -\frac{n-3}{2}, \ldots, \frac{n-1}{2}$ the notation

$$C_\gamma = \begin{pmatrix} \left(1 - e^{\frac{2\pi i \gamma}{n}}\right)\mathbb{I}_{|X_1|} & 0 \\ 0 & \left(1 + e^{\frac{-2\pi i \gamma}{n}}\right)\mathbb{I}_{|X_2|} \end{pmatrix} C_{X_1 \cup X_2}. \qquad (31)$$

As in the case of the Rényi entropies, the relation to the correlation matrix in Eq. (30) can be used within two different approaches to access the asymptotics of Rényi negatvities. In the first approach, we consider the series expansion of Eq. (30),

$$\mathcal{E}^{(n)} = \sum_{s=1}^{\infty} \frac{(-1)^{s+1}}{s}\mathrm{Tr}\left[\left\{\prod_{\gamma = -\frac{n-1}{2}}^{\frac{n-1}{2}}(\mathbb{I} - C_\gamma) - \mathbb{I}\right\}^s\right], \qquad (32)$$

and observe that it reduces the computation to that of an arbitrary joint moment of the modified correlation matrices C_γ, that is, a joint moment of the form

$$\mathrm{Tr}\left[C_{\gamma_1}\ldots C_{\gamma_p}\right] = \int\limits_{[-\pi,\pi]^p} \frac{d^p k}{(2\pi)^p}\prod_{j=1}^p \widetilde{f}(k_j)\left[\left(1 - e^{\frac{2\pi i \gamma_j}{n}}\right)\sum_{m \in X_1}\langle m|k_{j-1}\rangle\langle k_j|m\rangle + \left(1 + e^{\frac{-2\pi i \gamma_j}{n}}\right)\sum_{m \in X_2}\langle m|k_{j-1}\rangle\langle k_j|m\rangle\right], \qquad (33)$$

with p being a positive integer. Eq. (33) bears clear resemblance to Eq. (25), and similarly its asymptotic form can be estimated in our case of interest using the SPA (see details in Subsec. V C). The second approach, which is analogous to the one that uses Eq. (26) in the case of the Rényi entropies, simply rewrites Eq. (30) as

$$\mathcal{E}^{(n)} = \sum_{\gamma = -\frac{n-1}{2}}^{\frac{n-1}{2}} \ln\det[\mathbb{I} - C_\gamma], \qquad (34)$$

where again the asymptotics of the determinants can be analytically calculated provided a certain structure of the modified correlation matrices C_γ.

Lastly, we mention that, for a Gaussian state, the PRMI between X_1 and X_2 (defined in Eq. (5)) can also be efficiently expressed using restricted two-point correlation matrices. Indeed, the PRMI can be written as [48]

$$\mathcal{D}^{(n)} = \frac{1}{n-1}\mathrm{Tr}\ln\left[(C_{X_1 \cup X_2})^n (C_{X_1} \oplus C_{X_2})^{1-n} \\ + (\mathbb{I} - C_{X_1 \cup X_2})^n (\mathbb{I} - C_{X_1} \oplus C_{X_2})^{1-n}\right]. \qquad (35)$$

Eq. (35) is somewhat similar in its form to Eq. (23) for the Rényi entropy and Eq. (29) for the Rényi negativity, and indeed all of these formulae provide efficient ways to numerically calculate the quantities that they represent. However, the fact that the matrices $C_{X_1 \cup X_2}$ and $C_{X_1} \oplus C_{X_2}$ in general do not commute makes it difficult to bring Eq. (35) to a form akin to Eq. (26) or Eq. (34), and thus hinders the direct use of the same asymptotic techniques.

2. *Long-range limit of two-point correlations*

Since we focus on sites outside of the impurity region (such that $|j|, |m| > m_0$), Eqs. (10) and (11) can be used to write down the matrix element in Eq. (22) explicitly. Furthermore, this explicit expression becomes simpler when considering its long-range limit, i.e., when taking $d_i/\ell_i \to \infty$ with $d_L - d_R$ kept fixed. As explained in Ref. [19], we may use the Riemann-Lebesgue lemma to omit contributions to the matrix element that vanish in this limit, since they correspond to Fourier components with a diverging index. The two-point correlation

function is then given by

$$
\left\langle c_j^\dagger c_m \right\rangle \longrightarrow
\begin{cases}
\int_{-\pi}^0 \frac{dk}{2\pi}\, \widetilde{f}(k)\, e^{-i(j-m)k} + \int_0^\pi \frac{dk}{2\pi} \left[\widetilde{f}(k)\, \mathcal{T}(k) + \widetilde{f}(-k)\, \mathcal{R}(k) \right] e^{-i(j-m)k} & j,m \in A_R, \\
\int_{-\pi}^0 \frac{dk}{2\pi}\, \widetilde{f}(-k)\, e^{i(j-m)k} + \int_0^\pi \frac{dk}{2\pi} \left[\widetilde{f}(-k)\, \mathcal{T}(k) + \widetilde{f}(k)\, \mathcal{R}(k) \right] e^{i(j-m)k} & j,m \in A_L, \\
\int_0^\pi \frac{dk}{2\pi} \left[\widetilde{f}(k)\, t_L^*(k)\, r_L(k) + \widetilde{f}(-k)\, t_R(k)\, r_R^*(k) \right] e^{-i(j+m)k} & m \in A_L \text{ and } j \in A_R, \\
\int_0^\pi \frac{dk}{2\pi} \left[\widetilde{f}(k)\, t_L(k)\, r_L^*(k) + \widetilde{f}(-k)\, t_R^*(k)\, r_R(k) \right] e^{i(j+m)k} & j \in A_L \text{ and } m \in A_R.
\end{cases}
\tag{36}
$$

The analytical results presented in Sec. IV depend on d_L and d_R only through $d_L - d_R$, and in particular hold in the long-range limit, a fact which arguably constitutes the most remarkable aspect of our results. Accordingly, the numerical results to which we compared them in Sec. IV (see Figs. 2–4) were computed using two-point correlation matrices with their entries taken to the long-range limit given in Eq. (36). The exact diagonalization of the appropriate restricted correlation matrices allows to directly use the $n \to 1$ limits of Eqs. (23) and (29), as well as Eq. (35), to numerically compute entanglement entropies, the fermionic negativity and the PRMI. Moreover, the simplified correlation structure of Eq. (36) turns out to be essential for a central step in our analytical derivation, even though this derivation begins from the full expression in Eq. (22) for the two-point correlation function; we elaborate on this point in the following subsections.

B. Asymptotics of Rényi entropies

1. Entropies of A_L and A_R

In deriving the asymptotic form of the Rényi entropies for the two intervals A_L and A_R, we will rely on their relation with correlation matrix moments, which was introduced in Subsec. V A. Following the same methodology as the one that guided the analysis in Ref. [19], we substitute the eigenstate wavefunctions in Eqs. (10) and (11) into the expression for the correlation matrix moment given in Eq. (25). We employ the identity

$$
\sum_{m=r+1}^{r+s} \exp[im\,(k_{j-1} - k_j)] = s\, \mathcal{W}_r\!\left(\frac{k_{j-1} - k_j}{2} \right)
$$
$$
\times \int_0^1 d\xi \, \exp[is\,(k_{j-1} - k_j)\,\xi],
\tag{37}
$$

where we defined $\mathcal{W}_r(x) = \frac{1}{\sin x} x e^{i(2r+1)x}$, in order to bring the pth correlation matrix moment to the general

form

$$
\mathrm{Tr}[(C_{A_i})^p] = \sum_{\vec{\tau}, \vec{\sigma} \in \{0,1\}^{\otimes p}} \mathcal{G}(\vec{\tau}, \vec{\sigma}),
\tag{38}
$$

with

$$
\mathcal{G}(\vec{\tau}, \vec{\sigma}) = \ell_i{}^p \int\limits_{[-\pi,\pi]^p} \frac{d^p k}{(2\pi)^p} \int\limits_{[0,1]^p} d^p \xi \, g_{\vec{\tau},\vec{\sigma}}\!\left(\vec{k} \right)
$$
$$
\times \exp\left[i\ell_i \sum_{j=1}^p \left((-1)^{\tau_{j-1}} k_{j-1} - (-1)^{\sigma_j} k_j \right) \xi_j \right].
\tag{39}
$$

The particular forms of the functions $g_{\vec{\tau},\vec{\sigma}}$ depend on the scattering matrix associated with the impurity, as well as on the occupation factor $\widetilde{f}(k)$ associated with the reservoirs. Importantly, however, these functions are independent of ℓ_i.

In Ref. [19] we performed the asymptotic analysis of moments that were brought to the same form as in Eq. (38). This was done by applying to the integrals in Eq. (39) the SPA, according to which leading-order contributions arise from stationary points of the function appearing inside the exponent. There, we showed that in Eq. (38) only the terms with $\vec{\tau} = \vec{\sigma}$ may have a leading-order $\mathcal{O}(\ell_i)$ contribution to the moment, whereas terms with $\vec{\tau} \neq \vec{\sigma}$ have an $\mathcal{O}(\ell_i{}^0)$ contribution at most. The leading-order asymptotics is furthermore given by the formula

$$
\mathrm{Tr}[(C_{A_i})^p]
$$
$$
\sim \ell_i \int_{-\pi}^\pi \frac{dk}{2\pi} \sum_{\vec{\sigma} \in \{0,1\}^{\otimes p}} g_{\vec{\sigma},\vec{\sigma}}\!\left(k, (-1)^{\sigma_1 + \sigma_2} k, \ldots, (-1)^{\sigma_1 + \sigma_p} k \right),
\tag{40}
$$

which we can then express more explicitly using the particular functions $g_{\vec{\sigma},\vec{\sigma}}$ that satisfy the equality in Eq. (38). In Appendix A we go through the details of the computation, arriving at the following asymptotic

formulae:

$$\mathrm{Tr}[(C_{A_L})^p] \sim \ell_L \bigg[\int_0^\pi \frac{dk}{2\pi} \left(f_L(k)\right)^p$$

$$+ \int_0^\pi \frac{dk}{2\pi} \left(\mathcal{R}(k)\,f_L(k) + \mathcal{T}(k)\,f_R(k)\right)^p \bigg],$$

$$\mathrm{Tr}[(C_{A_R})^p] \sim \ell_R \bigg[\int_0^\pi \frac{dk}{2\pi} \left(f_R(k)\right)^p$$

$$+ \int_0^\pi \frac{dk}{2\pi} \left(\mathcal{T}(k)\,f_L(k) + \mathcal{R}(k)\,f_R(k)\right)^p \bigg]. \quad (41)$$

Finally, by substituting Eq. (41) into the power series expansion in Eq. (24), we obtain the following expressions for the Rényi entropies of A_L and A_R:

$$S_{A_L}^{(n)} \sim \frac{\ell_L}{1-n} \int_0^\pi \frac{dk}{2\pi} \bigg\{ \ln[(f_L)^n + (1-f_L)^n]$$

$$+ \ln[(\mathcal{R}f_L + \mathcal{T}f_R)^n + (1 - \mathcal{R}f_L - \mathcal{T}f_R)^n] \bigg\},$$

$$S_{A_R}^{(n)} \sim \frac{\ell_R}{1-n} \int_0^\pi \frac{dk}{2\pi} \bigg\{ \ln[(f_R)^n + (1-f_R)^n]$$

$$+ \ln[(\mathcal{T}f_L + \mathcal{R}f_R)^n + (1 - \mathcal{T}f_L - \mathcal{R}f_R)^n] \bigg\}. \quad (42)$$

2. Entropies of $A_L \cup A_R$

For convenience, we introduce here the notations $A = A_L \cup A_R$ and $\Delta\ell_i = \ell_i - \ell_{\mathrm{mirror}}$ $(i = L, R)$. Similarly to the case of the intervals A_L and A_R, the Rényi entropies of their union A can be computed by using the SPA to produce a general asymptotic expression for an integer moment of C_A, and by subsequently summing the power series in Eq. (24). The application of the SPA in this case, however, is considerably more intricate technically. Instead, we choose to rely on the SPA only to prove a simple relation between moments of C_A and moments of other restricted correlation matrices, a relation that leads to a useful decomposition of Rényi entropies of A.

In Appendix B we employ the SPA (essentially repeating an argument that we originally introduced in Ref. [19]) to show that, to a leading order, the moments of C_A can be decomposed into a sum of independent contributions in the form

$$\mathrm{Tr}[(C_A)^p] \sim \frac{\Delta\ell_L}{\ell_L} \mathrm{Tr}[(C_{A_L})^p] + \frac{\Delta\ell_R}{\ell_R} \mathrm{Tr}[(C_{A_R})^p]$$

$$+ \mathrm{Tr}[(C_{\mathrm{mirror}})^p], \quad (43)$$

where C_{mirror} is the restricted two-point correlation matrix of the subsystem $A_{\mathrm{mirror}} = \left(A_L \cap \bar{A}_R\right) \cup \left(\bar{A}_L \cap A_R\right)$,

i.e., the subsystem containing all sites in A_L that have mirroring sites in A_R and vice versa. For the first two moments appearing in the right-hand side of Eq. (43) we can use the result of Eq. (41), while a separate treatment is required for the moment of C_{mirror}.

The matrix C_{mirror} is of size $2\ell_{\mathrm{mirror}} \times 2\ell_{\mathrm{mirror}}$, and, as already mentioned, its moment can be estimated asymptotically for $\ell_{\mathrm{mirror}} \gg 1$ using the SPA, as was indeed done in Ref. [19] for the zero-temperature case. There is, however, an alternative approach that simplifies the calculation. The SPA analysis presented in Appendix B shows that, to a leading order, the moment of C_{mirror} is independent of $\max\{d_L, d_R\}$, which determines the absolute distance of the mirroring sites from the impurity region. This implies that we may take the limit $d_i \to \infty$ (with $d_L - d_R$ kept fixed) and the leading-order value of the moment will remain the same. Since this is true for any moment of C_{mirror}, it is true (by virtue of Eq. (24)) also for the Rényi entropies of A_{mirror}. In other words, Eqs. (24) and (43) allow us to write

$$S_A^{(n)} \sim \frac{\Delta\ell_L}{\ell_L} S_{A_L}^{(n)} + \frac{\Delta\ell_R}{\ell_R} S_{A_R}^{(n)} + S_{\mathrm{mirror}}^{(n)}, \quad (44)$$

with $S_{\mathrm{mirror}}^{(n)}$ designating the nth Rényi entropy of A_{mirror}, and to regard A_{mirror} as the union of two mirroring intervals that are infinitely far apart.

Following this reasoning, we can invoke the long-range limit of the two-point correlation function given in Eq. (36), which leads to a simplified structure of C_{mirror}. Expressing the relation between $S_{\mathrm{mirror}}^{(n)}$ and C_{mirror} using Eq. (26), this simplified structure enables the use of a powerful asymptotic technique. Indeed, using Eq. (36) we can arrange the long-range limit of C_{mirror} in the form of $\ell_{\mathrm{mirror}} \times \ell_{\mathrm{mirror}}$ blocks, each of size 2×2, with the entries of the block $\Phi^{(j,m)}$ $(j, m = 1, \ldots, \ell_{\mathrm{mirror}})$ depending only on the difference $j - m$; in that form, C_{mirror} is a block-Toeplitz matrix. The explicit form of the block $\Phi^{(j,m)}$ can be conveniently written as

$$\Phi^{(j,m)} = \int_{-\pi}^\pi \frac{dk}{2\pi} \Phi(k)\, e^{-i(j-m)k}, \quad (45)$$

where the entries of the 2×2 block symbol $\Phi(k)$ are given by

$$\Phi_{11} = \begin{cases} \widetilde{f}(-k) & -\pi < k < 0, \\ \widetilde{f}(-k)\,\mathcal{T}(k) + \widetilde{f}(k)\,\mathcal{R}(k) & 0 < k < \pi, \end{cases}$$

$$\Phi_{22} = \begin{cases} \widetilde{f}(k) & -\pi < k < 0, \\ \widetilde{f}(k)\,\mathcal{T}(k) + \widetilde{f}(-k)\,\mathcal{R}(k) & 0 < k < \pi, \end{cases}$$

$$\Phi_{12} = \begin{cases} 0 & -\pi < k < 0, \\ \left(\widetilde{f}(k) - \widetilde{f}(-k)\right) t_L(k)\, r_L^*(k) & 0 < k < \pi, \end{cases}$$

$$(46)$$

and $\Phi_{21} = \Phi_{12}^*$. Note that we used the fact that $t_R^* r_R = -t_L r_L^*$ due to the unitarity of the scattering matrix.

Next, we observe that in each determinant featured in Eq. (26) appears a block-Toeplitz matrix with the block symbol $\mathbb{I}_2 + \left(e^{2\pi i\gamma/n} - 1\right)\Phi$. The Szegö-Widom formula [65] states that, given a block-Toeplitz matrix $T_\ell[\Psi]$ defined by a continuous block symbol $\Psi(k)$ and comprised of $\ell \times \ell$ blocks, the leading-order large-ℓ asymptotics of its determinant is given by

$$\ln \det T_\ell[\Psi] \sim \ell \int_{-\pi}^{\pi} \frac{dk}{2\pi} \ln \det \Psi(k). \qquad (47)$$

Accordingly, we find that

$$\ln \det\left[\mathbb{I} + \left(e^{2\pi i\gamma/n} - 1\right) C_{\mathrm{mirror}}\right]$$
$$\sim \ell_{\mathrm{mirror}} \int_{-\pi}^{\pi} \frac{dk}{2\pi} \ln \det\left[\mathbb{I}_2 + \left(e^{2\pi i\gamma/n} - 1\right)\Phi(k)\right]$$
$$= \ell_{\mathrm{mirror}} \int_{-\pi}^{\pi} \frac{dk}{\pi} \ln\left[1 + \left(e^{2\pi i\gamma/n} - 1\right)\widetilde{f}(k)\right], \qquad (48)$$

and then, by summing over the index γ in Eq. (26), we obtain

$$S_{\mathrm{mirror}}^{(n)} \sim \frac{\ell_{\mathrm{mirror}}}{1-n} \int_{-\pi}^{\pi} \frac{dk}{\pi} \ln\left[\left(\widetilde{f}(k)\right)^n + \left(1 - \widetilde{f}(k)\right)^n\right]. \qquad (49)$$

Finally, combining Eqs. (42), (44) and (49), we may write the Rényi entropies of subsystem A as

$$S_A^{(n)} \sim \frac{\ell_L + \ell_{\mathrm{mirror}}}{1-n} \int_0^{\pi}\frac{dk}{2\pi} \ln[(f_L)^n + (1-f_L)^n]$$
$$+ \frac{\ell_R + \ell_{\mathrm{mirror}}}{1-n} \int_0^{\pi}\frac{dk}{2\pi} \ln[(f_R)^n + (1-f_R)^n]$$
$$+ \frac{\Delta\ell_L}{1-n} \int_0^{\pi}\frac{dk}{2\pi} \ln[(\mathcal{R}f_L + \mathcal{T}f_R)^n + (1-\mathcal{R}f_L - \mathcal{T}f_R)^n]$$
$$+ \frac{\Delta\ell_R}{1-n} \int_0^{\pi}\frac{dk}{2\pi} \ln[(\mathcal{T}f_L + \mathcal{R}f_R)^n + (1-\mathcal{T}f_L - \mathcal{R}f_R)^n]. \qquad (50)$$

Eqs. (42) and (50), when combined, lead to the expression in Eq. (16) for the RMI.

We conclude this part by noting that the approach we took to compute the entropies of A can be similarly used for the computation of the entropies of A_L and A_R. That is, instead of using the SPA throughout the entire computation – estimating exactly the correlation matrix moments and then summing the power series in Eq. (24) – we can use the SPA only to show that $S_{A_i}^{(n)}$ is independent of d_i to a leading order. Then, we can rely on

this fact to compute $S_{A_i}^{(n)}$ through Eq. (26) by substituting the long-range limit of C_{A_i}, which is of a Toeplitz form, as can be checked via Eq. (36). The Szegö-Widom formula can therefore be used to complete the calculation. Nevertheless, the direct application of the SPA to the computation of correlation matrix moments is relatively simple in the case of A_L and A_R, and we chose to present these two different variations of our analytical methodology in order to emphasize its versatility.

C. Asymptotics of Rényi negativities

Here we address the calculation of the Rényi negativity $\mathcal{E}^{(n)}$, which yields upon analytic continuation the asymptotics of the negativity, reported in Eq. (19). The derivation of $\mathcal{E}^{(n)}$ largely parallels that of $S_A^{(n)}$ ($A = A_L \cup A_R$) discussed in Subsec. V B. We will again use the notation $\Delta\ell_i = \ell_i - \ell_{\mathrm{mirror}}$ ($i = L, R$).

In Subsec. V A we explained that the Rényi negativity $\mathcal{E}^{(n)}$ can be expressed as a series of joint moments of the form given in Eq. (33) (with X_1 and X_2 standing for A_L and A_R, respectively), such that by computing a general expression for these joint moments we can obtain an expression for $\mathcal{E}^{(n)}$. As we explain in Appendix B, a decomposition of the joint moments which is analogous to Eq. (43) (used in the computation of $S_A^{(n)}$) is possible here due to the same SPA argument. Within the steady state of interest and to a leading order, the joint moments satisfy

$$\mathrm{Tr}\left[C_{\gamma_1}\ldots C_{\gamma_p}\right] \sim \frac{\Delta\ell_L}{\ell_L}\left(\prod_{j=1}^{p}\left(1 - e^{\frac{2\pi i\gamma_j}{n}}\right)\right)\mathrm{Tr}[(C_{A_L})^p]$$
$$+ \frac{\Delta\ell_R}{\ell_R}\left(\prod_{j=1}^{p}\left(1 + e^{\frac{-2\pi i\gamma_j}{n}}\right)\right)\mathrm{Tr}[(C_{A_R})^p]$$
$$+ \mathrm{Tr}\left[C_{\mathrm{mirror},\gamma_1}\ldots C_{\mathrm{mirror},\gamma_p}\right], \qquad (51)$$

where $C_{\mathrm{mirror},\gamma}$ is a modified version of C_{mirror} (the latter was defined right below Eq. (43)), given by Eq. (31) with $X_1 = A_L \cap \bar{A}_R$ and $X_2 = \bar{A}_L \cap A_R$. Substituting Eq. (51) into the power series expansion of the Rényi negativity in Eq. (32), we find upon summation that

$$\mathcal{E}^{(n)} \sim (1-n)\left[\frac{\Delta\ell_L}{\ell_L}S_{A_L}^{(n)} + \frac{\Delta\ell_R}{\ell_R}S_{A_R}^{(n)}\right] + \mathcal{E}_{\mathrm{mirror}}^{(n)}, \qquad (52)$$

with $\mathcal{E}_{\mathrm{mirror}}^{(n)}$ standing for the negativity between the two mirroring intervals comprising A_{mirror}, i.e., $A_L \cap \bar{A}_R$ and $\bar{A}_L \cap A_R$.

Moreover, as with the moments of C_{mirror} (see the discussion following Eq. (43)), the argument laid out in Appendix B implies that joint moments of the matrices $C_{\mathrm{mirror},\gamma}$ are independent of the distance between $A_L \cap \bar{A}_R$ and $\bar{A}_L \cap A_R$, such that we may assume that this distance is much larger than ℓ_{mirror} and use the long-range limit of

the two-point correlation function (given in Eq. (36)) to express the entries of C_{mirror}. Consequently, the matrices $C_{\text{mirror},\gamma}$ can be written as block-Toeplitz matrices with $\ell_{\text{mirror}} \times \ell_{\text{mirror}}$ blocks of size 2×2 each. The associated block symbol is given by

$$\Phi_\gamma(k) = \begin{pmatrix} 1 - e^{\frac{2\pi i \gamma}{n}} & 0 \\ 0 & 1 + e^{\frac{-2\pi i \gamma}{n}} \end{pmatrix} \Phi(k), \qquad (53)$$

with Φ being the block symbol of C_{mirror}, the entries of which are given explicitly in Eq. (46).

We may now exploit the block-Toeplitz structure of the matrices $C_{\text{mirror},\gamma}$ to obtain the asymptotics of $\mathcal{E}^{(n)}_{\text{mirror}}$,

given the relation in Eq. (34) between these matrices and the Rényi negativity. Employing the Szegö-Widom formula of Eq. (47), in Appendix C we compute the leading-order asymptotics of $\ln \det[\mathbb{I} - C_{\text{mirror},\gamma}]$ and perform the summation over the index γ in Eq. (34), finding that

$$\mathcal{E}^{(n)}_{\text{mirror}} \sim \ell_{\text{mirror}} \int_{-\pi}^{\pi} \frac{dk}{2\pi} \ln\left[\left(\widetilde{f}(k)\right)^n + \left(1 - \widetilde{f}(k)\right)^n\right]$$

$$+ \ell_{\text{mirror}} \int_0^\pi \frac{dk}{2\pi} \ln \mathcal{Y}_n(k), \qquad (54)$$

where we defined

$$\mathcal{Y}_n = [\mathcal{T}f_L + \mathcal{R}f_R - f_L f_R]^n + [\mathcal{R}f_L + \mathcal{T}f_R - f_L f_R]^n + \left[\sqrt{\left[\frac{1 - f_L - f_R + 2f_L f_R}{2}\right]^2 + \mathcal{T}\mathcal{R}(f_L - f_R)^2} + \frac{1 - f_L - f_R}{2}\right]^n$$

$$+ \left[\sqrt{\left[\frac{1 - f_L - f_R + 2f_L f_R}{2}\right]^2 + \mathcal{T}\mathcal{R}(f_L - f_R)^2} - \frac{1 - f_L - f_R}{2}\right]^n. \qquad (55)$$

Finally, by combining Eqs. (52) and (54), we arrive at the desired expression for the Rényi negativity between A_L and A_R:

$$\mathcal{E}^{(n)} \sim \ell_{\text{mirror}} \int_0^\pi \frac{dk}{2\pi} \ln \mathcal{Y}_n + \ell_L \int_0^\pi \frac{dk}{2\pi} \ln[(f_L)^n + (1 - f_L)^n] + \ell_R \int_0^\pi \frac{dk}{2\pi} \ln[(f_R)^n + (1 - f_R)^n]$$

$$+ \Delta\ell_L \int_0^\pi \frac{dk}{2\pi} \ln[(\mathcal{R}f_L + \mathcal{T}f_R)^n + (1 - \mathcal{R}f_L - \mathcal{T}f_R)^n] + \Delta\ell_R \int_0^\pi \frac{dk}{2\pi} \ln[(\mathcal{T}f_L + \mathcal{R}f_R)^n + (1 - \mathcal{T}f_L - \mathcal{R}f_R)^n]. \quad (56)$$

The fermionic negativity in Eq. (19) is obtained by taking the $n \to 1$ limit of the above expression.

D. Asymptotics of Petz-Rényi mutual information

In this part, we briefly summarize the calculation leading to Eq. (17), which states the analytical form of the PRMI $\mathcal{D}^{(n)}$ between A_L and A_R. The derivation is more conjectural compared to those discussed in Subsecs. V B and V C, owing to the difficulty (which was already mentioned in Subsec. V A) in applying the same analytical techniques to the expression in Eq. (35) of the PRMI in terms of two-point correlation matrices. The validity of the final result is corroborated by its comparison to numerical results, presented in Fig. 4 and discussed at the end of Sec. IV.

Like in the case of Eqs. (24) and (32), Eq. (35) can be expanded to a power series, reducing the calculation of the PRMI to that of joint moments of C_A and $C_{A_L} \oplus C_{A_R}$.

By the same argument that is detailed in Appendix B, at the leading order these moments can be decomposed into independent contributions from A_{mirror}, $A_L \setminus \bar{A}_R$ and $A_R \setminus \bar{A}_L$; since the matrices C_A and $C_{A_L} \oplus C_{A_R}$ are identical when projected onto either $A_L \setminus \bar{A}_R$ or $A_R \setminus \bar{A}_L$, the contributions from these two subsystems fall off, leaving us with

$$\mathcal{D}^{(n)} \sim \frac{1}{n-1} \ln \det\left[(C_{\text{mirror}})^n \left(C_{A_L \cap \bar{A}_R} \oplus C_{\bar{A}_L \cap A_R}\right)^{1-n}\right.$$

$$\left. + (\mathbb{I} - C_{\text{mirror}})^n \left(\mathbb{I} - C_{A_L \cap \bar{A}_R} \oplus C_{\bar{A}_L \cap A_R}\right)^{1-n}\right]. \tag{57}$$

Furthermore, due to the same logic presented in Appendix B regarding similar moments of correlation matrices, $\mathcal{D}^{(n)}$ should be independent (at the leading order) of the distance between $A_L \cap \bar{A}_R$ and $\bar{A}_L \cap A_R$, meaning that we can regard this distance as infinite, as we have done in Subsecs. V B and V C. Then, recalling Eq. (36), we see that both C_{mirror} and $C_{A_L \cap \bar{A}_R} \oplus C_{\bar{A}_L \cap A_R}$ are of

a block-Toeplitz form: the former is represented by the block-symbol Φ given in Eq. (46), while the latter is represented by a block-symbol $\Phi_\times$ given by $(\Phi_\times)_{ij} = \delta_{ij}\Phi_{ij}$.

In general, a product of two block-Toeplitz matrices is not itself a block-Toeplitz matrix. This fact prevents us form directly using the Szegö-Widom formula of Eq. (47) to estimate the scaling of Eq. (57) (it is also what led us to first express Rényi entropies and negativities as in Eqs. (26) and (34), so that the Szegö-Widom formula could be in fact employed). Instead, we use a recent conjecture that generalizes the Szegö-Widom formula. Let $\Psi_1, \Upsilon_1, \ldots, \Psi_p, \Upsilon_p$ be block-symbols of the same size, and let $T_\ell[\Psi_j], T_\ell[\Upsilon_j]$ $(j = 1, \ldots, p)$ be the block-Toeplitz matrices generated by them (each comprised of ℓ^2 blocks). Then, it was conjectured in Ref. [62] that

$$\ln \det \left[\mathbb{I} + \prod_{j=1}^{p} T_\ell[\Psi_j] \left(T_\ell[\Upsilon_j] \right)^{-1} \right]$$

$$\sim \ell \int_{-\pi}^{\pi} \frac{dk}{2\pi} \ln \det \left[\mathbb{I} + \prod_{j=1}^{p} \Psi_j \Upsilon_j^{-1} \right]. \quad (58)$$

Applying this conjecture to Eq. (57), we obtain

$$\mathcal{D}^{(n)} \sim \frac{\ell_{\text{mirror}}}{n-1} \int_{-\pi}^{\pi} \frac{dk}{2\pi} \ln \det \left[(\Phi)^n (\Phi_\times)^{1-n} \right.$$

$$\left. + (\mathbb{I} - \Phi)^n (\mathbb{I} - \Phi_\times)^{1-n} \right]. \quad (59)$$

It is not difficult to express the integer powers of $\Phi(k)$ and $\Phi_\times(k)$: the latter is diagonal for all k, and the former is diagonal for $k < 0$, while for $k > 0$ one may check that

$$(\Phi)^n = \begin{pmatrix} \mathcal{R}f_L{}^n + \mathcal{T}f_R{}^n & t_L r_L^* \left(f_L{}^n - f_R{}^n \right) \\ t_L^* r_L \left(f_L{}^n - f_R{}^n \right) & \mathcal{T}f_L{}^n + \mathcal{R}f_R{}^n \end{pmatrix}. \quad (60)$$

Therefore, by substituting the explicit expressions for Φ and $\Phi_\times$ into Eq. (59), it is straightforward to finally arrive at Eq. (17).

VI. SUMMARY AND OUTLOOK

This paper advances our program for exploring the correlation and entanglement structure of nonequilibrium steady states, focusing on the steady state of biased free fermions in one dimension in the presence of a homogeneity-breaking impurity. The results reported here extend those of Ref. [19], by showing that the phenomenon of stationary volume-law long-range entanglement arises not only for a chemical potential bias at zero temperature, but more generally given any difference between the equilibrium distributions of the two edge reservoirs that impose the nonequilibrium bias. In particular, this strong long-range entanglement is found to be robust even at finite temperatures. We offered an intuitive explanation for the source of the phenomenon, attributing

it to the coherence between the transmitted and reflected parts of wavepackets occupying each single-particle energy mode, provided that the two scattering states that correspond to the same energy are not simultaneously occupied.

Our analysis produced exact leading-order asymptotic expressions for various bipartite quantum information quantities, computed for two subsystems located on opposite sides of the impurity. Most notably, this includes exact formulae for the fermionic negativity (quantifying entanglement) and the mutual information (quantifying the combined classical and quantum correlations) between the two subsystems. Additional analytical expressions were derived for Rényi negativities, the Rényi mutual information, and the Petz-Rényi mutual information, where the latter is itself a proper measure of inter-subsystem correlations. All of these analytical results were obtained without assuming a specific structure of the impurity (other than requiring that it will be quadratic and charge-conserving), and are expressed solely in terms of the scattering probabilities associated with the impurity, and of the equilibrium energy distributions of the reservoirs.

The exact expressions for the volume-law terms of the negativity and the mutual information vanish either in the absence of the nonequilibrium bias, or if the impurity perfectly transmits or perfectly reflects each particle, but are positive otherwise. In this sense, the model we studied can be regarded as a minimal model giving rise to volume-law long-range entanglement, seeing that the bias and the locally broken homogeneity, which are essentially the defining features of the model, constitute the necessary and sufficient conditions for the phenomenon. The analytical expression for the mutual information also nicely captures the local nonequilibrium energy distribution that arises due to the combination of the bias and the scattering, as indeed required in order to violate the thermal equilibrium area law of the mutual information.

Furthermore, we found a proportionality relation (at the leading volume-law order) between the negativity, the $\frac{1}{2}$-RMI and the $\frac{5}{4}$-PRMI, which holds at zero temperature but breaks down otherwise. As we elaborated in Sec. IV, this relation indicates that the strong long-range correlations are entirely of a quantum coherent nature, while its breakdown signals a significant contribution to these correlations beyond what is quantified by the negativity. Like in other free-fermion models where this relation was observed to break down [26, 60, 61], this effect occurs in our case when the global state of the system is mixed; this property is however insufficient in general, see e.g. Ref. [66]. The precise conditions for the breakdown of this proportionality relation, as well as its operational meaning, remain to the best of our knowledge subjects of open questions.

We stress that while, for concreteness, we treated a particular choice for the energy dispersion relation, our analysis does not depend on it, and should be applicable to any gapless free-fermion model. Similarly, given that

our results are expressed directly using the energy distribution functions of the edge reservoirs, more general forms can be chosen for these distributions, and they need not necessarily be of the Fermi-Dirac form.

Along with the physical insights produced by this work, it also showcases the versatility of the analytical machinery that we put forward in Ref. [19], and used here to generalize our original results. It is reasonable to expect that the same method would be useful for similar investigations concerning different noninteracting fermionic models. This method should also be appropriate for calculations of quantities that address the interplay of charge conservation with steady-state correlations across the impurity, namely the full counting statistics [67–69] and charge-resolved entanglement measures [70–77].

Another worthwhile pursuit could be the analytical study of subleading corrections beyond the volume-law asymptotics derived here. Indeed, such corrections often have universal forms that disclose fundamental physical attributes of the system in question [22, 78, 79]. In Ref. [80] we already derived the exact forms of the logarithmic corrections to the leading terms of correlation measures in the case of zero temperature, finding that they can become comparable to the volume-law terms when the chemical-potential bias is small enough. While the method used in Ref. [80] is not immediately suitable to tackle the case of finite temperatures, we note that the zero-temperature exact expressions are similar in their structure to the asymptotic expressions for the same quantities in ground states of conformal field theories [24, 81]. Thus, the well-known finite-temperature scaling in the case of the latter (which is logarithmic in the temperature) could presumably provide guidance in calculating subleading contributions in the case of the nonequilibrium steady state.

On a more ambitious note, we reiterate the resemblance between the stationary behavior of the MI and the negativity studied here and the transient long-range peak of these quantities following a nonequilibrium quench of closed integrable systems [7, 10–12]. Even though the latter include interacting models, this transient phenomenon is explained by the quasiparticle picture, which portrays information spreading as a process mediated by independent pairs of counter-propagating quasiparticles [5, 82]. It is tempting to conjecture that the long-range volume-law scaling we reported here, considering an open biased system, would also apply to integrable interacting

systems containing an impurity [38]. The success or failure of this conjecture could offer a glimpse into the limits of validity of the quasiparticle picture [83, 84].

The effects of integrability breaking, which in the case of the quench scenario destroys the long-range coherence of information propagation [12], are likewise an exciting prospective subject for future research. Integrability could be broken either by the impurity [85–87] or in the bulk of the model, and each case could potentially lead to a quantitatively different scaling of quantum correlation measures. The impact of decoherence and dissipation on the phenomenon that we described certainly merits a separate consideration as well [31, 88, 89], as do possible similar studies applied to steady states of conformal field theories [37, 90, 91]. Finally, we note that these various questions can be studied experimentally using any quantum simulation platform that offers local density resolution [41, 92, 93].

Appendix A: Moments of correlation matrices restricted to A_L and A_R

In this appendix we detail the method used to compute integer moments of C_{A_L} and C_{A_R} (the two-point correlation matrices restricted to A_L and A_R, respectively), leading to Eq. (41). The method relies on the stationary phase approximation (SPA) [64], and the calculation is almost identical to the one performed in the zero-temperature case, which was detailed in Ref. [19]; we provide the details of the calculation in the more general case for the sake of completeness. We focus our discussion on moments of C_{A_R}, with the corresponding computation for C_{A_L} being virtually equivalent.

We begin by introducing the following notations:

$$\Xi^{00}(k_{j-1}, k_j) = t_L(|k_{j-1}|)\, t_L^*(|k_j|)\, \mathcal{W}_R\left(\frac{k_{j-1} - k_j}{2}\right) \int_0^1 d\xi\, e^{i\ell_R(k_{j-1} - k_j)\xi},$$

$$\Xi^{11}(k_{j-1}, k_j) = \int_0^1 d\xi \left\{ \mathcal{W}_R\left(\frac{k_j - k_{j-1}}{2}\right) e^{i\ell_R(k_j - k_{j-1})\xi} + r_R(|k_{j-1}|)\, r_R^*(|k_j|)\, \mathcal{W}_R\left(\frac{k_{j-1} - k_j}{2}\right) e^{i\ell_R(k_{j-1} - k_j)\xi} \right\}$$

$$+ \int_0^1 d\xi \left\{ r_R^*(|k_j|)\, \mathcal{W}_R\left(\frac{-k_{j-1} - k_j}{2}\right) e^{-i\ell_R(k_{j-1} + k_j)\xi} + r_R(|k_{j-1}|)\, \mathcal{W}_R\left(\frac{k_{j-1} + k_j}{2}\right) e^{i\ell_R(k_{j-1} + k_j)\xi} \right\},$$

$$\Xi^{01}(k_{j-1}, k_j) = t_L(|k_{j-1}|) \int_0^1 d\xi \left\{ \mathcal{W}_R\left(\frac{k_{j-1} + k_j}{2}\right) e^{i\ell_R(k_{j-1} + k_j)\xi} + r_R^*(|k_j|)\, \mathcal{W}_R\left(\frac{k_{j-1} - k_j}{2}\right) e^{i\ell_R(k_{j-1} - k_j)\xi} \right\}, \quad \text{(A1)}$$

where $\mathcal{W}_R(x) = \mathcal{W}_{m_0 + d_R}(x)$ (recall the definition of $\mathcal{W}_r$, given just below Eq. (37)). We also define the functions

$$\widetilde{\Xi}^{00}(k_{j-1}, k_j) = \mathcal{T}(|k_j|) \int_0^1 d\xi\, e^{i\ell_R(k_{j-1} - k_j)\xi},$$

$$\widetilde{\Xi}^{11}(k_{j-1}, k_j) = \int_0^1 d\xi \left\{ e^{i\ell_R(k_j - k_{j-1})\xi} \right.$$
$$\left. + \mathcal{R}(|k_j|)\, e^{i\ell_R(k_{j-1} - k_j)\xi} \right\},$$

$$\widetilde{\Xi}^{01}(k_{j-1}, k_j) = t_L(|k_j|)\, r_R^*(|k_j|) \int_0^1 d\xi\, e^{i\ell_R(k_{j-1} - k_j)\xi},$$

(A2)

as well as $\Xi^{10}(k_{j-1}, k_j) = \Xi^{01}(k_j, k_{j-1})^*$ and $\widetilde{\Xi}^{10}(k_{j-1}, k_j) = \widetilde{\Xi}^{01}(k_j, k_{j-1})^*$. Next, we substitute the eigenstate wavefunctions in Eqs. (10) and (11) into the general expression for a correlation matrix moment in Eq. (25). Using the identity given in Eq. (37), this yields

$$\mathrm{Tr}[(C_{A_R})^p] = \ell_R{}^p \int_{[-\pi, \pi]^p} \frac{d^p k}{(2\pi)^p} \prod_{j=1}^p \widetilde{f}(k_j)$$
$$\times \sum_{\vec{a} \in \{0,1\}^{\otimes p}} \prod_{j=1}^p \left[\Xi^{a_{j-1} a_j}\left(k_{a_{j-1}}, k_{a_j}\right) \Theta\left(k_{a_j}\right) \right],$$

(A3)

where $\Theta(x)$ is the Heaviside step function, and we defined $k_{a_j} = (-1)^{a_j} k_j$. It is readily seen that Eq. (A3) can be cast in the general form given in Eq. (38), and therefore the result of Eq. (40), which stems from the SPA, can be directly applied to obtain the leading-order asymptotics of the correlation matrix moment.

Eq. (40) dictates that the summands $\mathcal{G}(\vec{\tau}, \vec{\sigma})$ in Eq. (38) that contribute to the leading order are only those with $\vec{\tau} = \vec{\sigma}$. Furthermore, it constrains the integration variable $\vec{k}$ in the integral expression for $\mathcal{G}(\vec{\sigma}, \vec{\sigma})$ (see Eq. (39)) to a subdomain where $k_{\sigma_{j-1}} = k_{\sigma_j}$ for $1 \leq j \leq p$. This constraint entails a considerable simplification of Eq. (A3) when considering it only up to the leading order. Indeed, the aforementioned integration subdomain would eventually correspond to the vanishing of the terms $k_{j-1} \pm k_j$ appearing inside the exponents in Eq. (A1). However, the term $k_{j-1} + k_j$ does not vanish if $k_{j-1}, k_j > 0$, while each term $\Xi^{a_{j-1} a_j}\left(k_{a_{j-1}}, k_{a_j}\right) \Theta\left(k_{a_{j-1}}\right) \Theta\left(k_{a_j}\right)$ in Eq. (A3) vanishes due to the step functions unless $k_{a_{j-1}}, k_{a_j} > 0$. We may therefore omit from the functions defined in Eq. (A1) the integrals where $k_{j-1} + k_j$ appears in the exponent. Due to the same subdomain constraint, we may also substitute $k_{j-1} = k_j$ into all ξ-independent factors appearing in Eq. (A1). This step is captured by replacing in Eq. (A3) the functions $\Xi^{a_{j-1} a_j}$ with the functions $\widetilde{\Xi}^{a_{j-1} a_j}$, where the latter were defined in Eq. (A2) (note that we used the fact that $\mathcal{W}_r(0) = 1$).

Therefore, to a leading order we may write

$$\mathrm{Tr}[(C_{A_R})^p] \sim \ell_R{}^p \int_{[-\pi, \pi]^p} \frac{d^p k}{(2\pi)^p} \prod_{j=1}^p \widetilde{f}(k_j)$$
$$\times \sum_{\vec{a} \in \{0,1\}^{\otimes p}} \prod_{j=1}^p \left[\widetilde{\Xi}^{a_{j-1} a_j}\left(k_{a_{j-1}}, k_{a_j}\right) \Theta\left(k_{a_j}\right) \right].$$

(A4)

Casting this in the form of Eq. (38) and omitting integrals $\mathcal{G}(\vec{\tau}, \vec{\sigma})$ with $\vec{\tau} \neq \vec{\sigma}$, we have

$$\text{Tr}[(C_{A_R})^p] \sim \ell_R{}^p \int\limits_{[-\pi,0]^p} \frac{d^p k}{(2\pi)^p} \int\limits_{[0,1]^p} d^p \xi \prod_{j=1}^p \widetilde{f}(k_j)\, e^{i\ell_R(k_{j-1}-k_j)\xi_j} + \ell_R{}^p \int\limits_{[-\pi,\pi]^p} \frac{d^p k}{(2\pi)^p} \prod_{j=1}^p \widetilde{f}(k_j)$$

$$\times \int\limits_{[0,1]^p} d^p \xi \sum_{\overrightarrow{a}\in\{0,1\}^{\otimes p}} \prod_{j=1}^p \left\{ \Theta(k_{a_j}) \exp\left[i\ell_R(k_{a_{j-1}}-k_{a_j})\xi_j\right] \frac{1+(-1)^{a_j}\left[\mathcal{T}(k_{a_j})-\mathcal{R}(k_{a_j})\right]}{2} \right\}, \qquad (A5)$$

which then, using Eq. (40), leads to the result

$$\text{Tr}[(C_{A_R})^p] \sim \ell_R \int\limits_{-\pi}^{0} \frac{dk}{2\pi} \left(\widetilde{f}(k)\right)^p$$

$$+ \ell_R \int\limits_{0}^{\pi} \frac{dk}{2\pi} \left(\mathcal{T}(k)\,\widetilde{f}(k) + \mathcal{R}(k)\,\widetilde{f}(-k)\right)^p . \tag{A6}$$

As mentioned before, the calculation of the moments of C_{A_L} is equivalent, yielding a result similar to Eq. (A6), up to replacing ℓ_R with ℓ_L and $\widetilde{f}(k)$ with $\widetilde{f}(-k)$. This can also be written in the form given in Eq. (41).

Appendix B: Stationary phase approximation for moments of correlation matrices restricted to A

In this appendix, we lay out the argument that leads to the decomposition of correlation matrix moments given in Eqs. (43) and (51) for the subsystem $A = A_L \cup A_R$. For this purpose, we assume that the length scales $\Delta\ell_L$, $\Delta\ell_R$ and ℓ_{mirror} are all large, and that they scale linearly with the same large parameter ℓ. We define $\Delta\ell_- = |d_L - d_R|$ and $\Delta\ell_+ = |\ell_L + d_L - \ell_R - d_R|$; note that $\Delta\ell_\pm$ correspond to $\Delta\ell_L$ and $\Delta\ell_R$, with the specific correspondence depending on the relative positions of $\bar{A}_L$ (the mirror image of A_L) and A_R. We also write $\ell_{\text{mirror}} = \alpha_{\text{m}}\ell$ and $\Delta\ell_\pm = \alpha_\pm \ell$.

The core of the argument is related to the large-ℓ leading-order asymptotics of integrals of the following form (adopting the notation $k_{a_j} = (-1)^{a_j} k_j$ from Appendix A):

$$\mathcal{G}_{\overrightarrow{\alpha}}(\overrightarrow{\tau}, \overrightarrow{\sigma}) = \left[\prod_{j=1}^p (\alpha_j \ell)\right] \int\limits_{[-\pi,\pi]^p} \frac{d^p k}{(2\pi)^p} \int\limits_{[0,1]^p} d^p \xi\, g\left(\overrightarrow{k}\right)$$

$$\times \exp\left[i\ell \sum_{j=1}^p \left(k_{\tau_{j-1}} - k_{\sigma_j}\right)\left(\alpha_j \xi_j + \beta_j\right)\right]. \tag{B1}$$

Here, $(\alpha_j, \beta_j) \in \{(\alpha_-, 0), (\alpha_{\text{m}}, \alpha_-), (\alpha_+, \alpha_- + \alpha_{\text{m}})\}$ for each $1 \le j \le p$, and the form of the function g might depend on $\overrightarrow{\tau}$, $\overrightarrow{\sigma}$ or $\overrightarrow{\alpha}$, but not on ℓ. In Ref. [19] we

have found, based on the SPA, that an integral of the form of $\mathcal{G}_{\overrightarrow{\alpha}}(\overrightarrow{\tau}, \overrightarrow{\sigma})$ can scale linearly with ℓ only if $\alpha_1 = \alpha_2 = \ldots = \alpha_p$; otherwise, $\lim_{\ell\to\infty} \mathcal{G}_{\overrightarrow{\alpha}}/\ell = 0$, even when $\overrightarrow{\tau} = \overrightarrow{\sigma}$. Intuitively, this happens because when $\overrightarrow{\tau} = \overrightarrow{\sigma}$ and all the α_j are the same, then the stationary points of the function inside the exponent in Eq. (B1) constitute the entire line $\xi_1 = \xi_2 = \ldots = \xi_p$, while they are reduced, at most, to an isolated point in $\overrightarrow{\xi}$-space if $\alpha_{j-1} \ne \alpha_j$.

Consider now the integer moments of the matrix C_A, expressed as in Eq. (25). The sum over $m \in A$ in Eq. (25) can be split in the following way:

$$\sum_{m\in A} \langle m|k_{j-1}\rangle\langle k_j|m\rangle$$

$$= \sum_{m\in \bar{A}_L \cap A_R} \left[\langle -m|k_{j-1}\rangle\langle k_j|-m\rangle + \langle m|k_{j-1}\rangle\langle k_j|m\rangle\right]$$

$$+ \sum_{m\in \bar{A}_L \setminus A_R} \langle -m|k_{j-1}\rangle\langle k_j|-m\rangle + \sum_{m\in A_R \setminus \bar{A}_L} \langle m|k_{j-1}\rangle\langle k_j|m\rangle . \tag{B2}$$

Next, we define $d_- = \min\{d_L, d_R\}$, $d_+ = \max\{d_L, d_R\}$ and $\mathcal{W}_-(x) = \mathcal{W}_{m_0+d_-}(x)$ (recall the definition of $\mathcal{W}_r$, given just below Eq. (37)). After substituting the eigenstate wavefunctions of Eqs. (10)–(11) into the first sum on the right hand side of Eq. (B2), this sum can be brought to an integral form using the identity

$$\sum_{m=m_0+d_++1}^{m_0+d_++\ell_{\text{mirror}}} e^{im(k_{j-1}-k_j)} = \alpha_{\text{m}}\ell\, \mathcal{W}_-\left(\frac{k_{j-1}-k_j}{2}\right)$$

$$\times \int\limits_0^1 d\xi\, e^{i\ell(k_{j-1}-k_j)(\alpha_{\text{m}}\xi+\alpha_-)}, \tag{B3}$$

which is equivalent to Eq. (37). Similarly, for the two other sums appearing on the right hand side of Eq. (B2), we may use Eq. (37) directly with $r = m_0 + d_-$ and $s = \Delta\ell_-$, as well as the fact that

$$\sum_{m=m_0+d_++\ell_{\text{mirror}}+1}^{m_0+d_++\ell_{\text{mirror}}+\Delta\ell_+} e^{im(k_{j-1}-k_j)}$$

$$= \alpha_+\ell\, \mathcal{W}_-\left(\frac{k_{j-1}-k_j}{2}\right) \int\limits_0^1 d\xi\, e^{i\ell(k_{j-1}-k_j)(\alpha_+\xi+\alpha_-+\alpha_{\text{m}})}. \tag{B4}$$

In all, it is clear that the substitution of the wavefunctions from Eqs. (10)–(11) into the expression in Eq. (25) leads to the pth moment of C_A being written as a sum of integrals of the form given in Eq. (B1). The observation

we cited from Ref. [19] means that we can ignore all of the integrals where the entries of $\overrightarrow{\alpha}$ are not all the same, such that to a leading order we have

$$
\begin{aligned}
\mathrm{Tr}[(C_A)^p] \sim &\int\limits_{[-\pi,\pi]^p} \frac{d^p k}{(2\pi)^p} \prod_{j=1}^{p} \widetilde{f}(k_j) \left[\sum_{m \in \bar{A}_L \cap A_R} [\langle -m|k_{j-1}\rangle\langle k_j|-m\rangle + \langle m|k_{j-1}\rangle\langle k_j|m\rangle] \right] \\
&+ \int\limits_{[-\pi,\pi]^p} \frac{d^p k}{(2\pi)^p} \prod_{j=1}^{p} \widetilde{f}(k_j) \left[\sum_{m \in \bar{A}_L \setminus A_R} \langle -m|k_{j-1}\rangle\langle k_j|-m\rangle \right] + \int\limits_{[-\pi,\pi]^p} \frac{d^p k}{(2\pi)^p} \prod_{j=1}^{p} \widetilde{f}(k_j) \left[\sum_{m \in A_R \setminus \bar{A}_L} \langle m|k_{j-1}\rangle\langle k_j|m\rangle \right],
\end{aligned}
\tag{B5}
$$

or simply

$$
\begin{aligned}
\mathrm{Tr}[(C_A)^p] \sim \; &\mathrm{Tr}[(C_{\mathrm{mirror}})^p] \\
&+ \mathrm{Tr}\left[\left(C_{A_L \setminus \bar{A}_R} \right)^p \right] + \mathrm{Tr}\left[\left(C_{A_R \setminus \bar{A}_L} \right)^p \right].
\end{aligned}
\tag{B6}
$$

Since $A_L \setminus \bar{A}_R$ and $A_R \setminus \bar{A}_L$ are just portions of A_L and A_R with lengths $\Delta \ell_L$ and $\Delta \ell_R$, respectively, and given that the correlation matrix moments of these subsystems scale linearly with their lengths, we have in fact arrived at Eq. (43).

Moreover, we may observe that the moment of C_{mirror} does not depend (to the leading order) on the absolute distances of the subsystems from the impurity. Indeed,

if we use the identity in Eq. (B3) when substituting the wavefunctions into the first integral in Eq. (B5), we see that the dependence on the distance enters only through the function $\mathcal{W}_-$. However, as we explained in Appendix A, the SPA always constrains the argument of that function to vanish in its contribution to the leading order term of the asymptotics. Since $\mathcal{W}_-(0) = 1$, we conclude that the leading order term does not depend on the distance.

Finally, we note that the argument that lead to Eq. (B5) can be applied also to the joint moments given in Eq. (33). Indeed, it is straightforward to check that by repeating the steps that were taken in the case of the moments of C_A, one obtains that, to a leading order,

$$
\begin{aligned}
\mathrm{Tr}\left[C_{\gamma_1} \ldots C_{\gamma_p} \right] \sim &\int\limits_{[-\pi,\pi]^p} \frac{d^p k}{(2\pi)^p} \prod_{j=1}^{p} \widetilde{f}(k_j) \left[\sum_{m \in \bar{A}_L \cap A_R} \left[\left(1 - e^{\frac{2\pi i \gamma_j}{n}} \right) \langle -m|k_{j-1}\rangle\langle k_j|-m\rangle + \left(1 + e^{\frac{-2\pi i \gamma_j}{n}} \right) \langle m|k_{j-1}\rangle\langle k_j|m\rangle \right] \right] \\
&+ \int\limits_{[-\pi,\pi]^p} \frac{d^p k}{(2\pi)^p} \prod_{j=1}^{p} \widetilde{f}(k_j) \left(1 - e^{\frac{2\pi i \gamma_j}{n}} \right) \left[\sum_{m \in \bar{A}_L \setminus A_R} \langle -m|k_{j-1}\rangle\langle k_j|-m\rangle \right] \\
&+ \int\limits_{[-\pi,\pi]^p} \frac{d^p k}{(2\pi)^p} \prod_{j=1}^{p} \widetilde{f}(k_j) \left(1 + e^{\frac{-2\pi i \gamma_j}{n}} \right) \left[\sum_{m \in A_R \setminus \bar{A}_L} \langle m|k_{j-1}\rangle\langle k_j|m\rangle \right].
\end{aligned}
\tag{B7}
$$

This yields Eq. (51), again by relying on the linear scaling with ℓ_i of moments of C_{A_i}. As in the case of the moments of C_{mirror}, the integral in the first row of Eq. (B7) is independent of the distance of the mirroring sites from the impurity, by virtue of the same SPA argument.

Appendix C: Rényi negativity from the Szegö-Widom formula

Here we delineate the derivation of Eq. (54), which states the asymptotic scaling of the Rényi negativity between two mirroring intervals of length ℓ_{mirror}, in the limit of infinite distance between them and the impurity.

We begin by using the block-Toeplitz structure of the

matrix $\mathbb{I} - C_{\mathrm{mirror},\gamma}$, which is generated by the block-symbol $\mathbb{I}_2 - \Phi_\gamma$, where Φ_γ is defined in Eq. (53). The

Szegö-Widom formula given in Eq. (47) yields the asymptotics of the determinant of this matrix:

$$\frac{\ln \det[\mathbb{I} - C_{\mathrm{mirror},\gamma}]}{\ell_{\mathrm{mirror}}} \sim \int_0^\pi \frac{dk}{2\pi} \left\{ \ln\left[1 - \left(1 - e^{\frac{2\pi i\gamma}{n}}\right) f_L\right] + \ln\left[1 - \left(1 + e^{\frac{-2\pi i\gamma}{n}}\right) f_R\right] + \ln\left[1 - \left(1 - e^{\frac{2\pi i\gamma}{n}}\right)(\mathcal{R}f_L + \mathcal{T}f_R) \right. \right.$$
$$\left. \left. - \left(1 + e^{\frac{-2\pi i\gamma}{n}}\right)(\mathcal{T}f_L + \mathcal{R}f_R) + \left(1 - e^{\frac{2\pi i\gamma}{n}}\right)\left(1 + e^{\frac{-2\pi i\gamma}{n}}\right) f_L f_R\right]\right\}. \tag{C1}$$

Now, using the expression in Eq. (34) for the Rényi negativity in terms of determinants, we obtain

$$\mathcal{E}_{\mathrm{mirror}}^{(n)} \sim \ell_{\mathrm{mirror}} \int_0^\pi \frac{dk}{2\pi} \left\{ \ln[(f_L)^n + (1 - f_L)^n] \right.$$
$$\left. + \ln[(f_R)^n + (1 - f_R)^n] + \ln \mathcal{X}_n(k) \right\}, \tag{C2}$$

where we introduced the notation

$$\mathcal{X}_n = \prod_{\gamma=-\frac{n-1}{2}}^{\frac{n-1}{2}} \left[1 - \left(1 - e^{\frac{2\pi i\gamma}{n}}\right)(\mathcal{R}f_L + \mathcal{T}f_R)\right.$$
$$- \left(1 + e^{\frac{-2\pi i\gamma}{n}}\right)(\mathcal{T}f_L + \mathcal{R}f_R)$$
$$\left. + \left(1 - e^{\frac{2\pi i\gamma}{n}}\right)\left(1 + e^{\frac{-2\pi i\gamma}{n}}\right) f_L f_R\right]. \tag{C3}$$

Comparing Eq. (C2) to Eq. (54), we observe that what remains to be done is to prove the equality $\mathcal{X}_n(k) = \mathcal{Y}_n(k)$, where the definition of the function $\mathcal{Y}_n$ appears in Eq. (55). To do so, we will temporarily stop viewing f_L, f_R and $\mathcal{T}$ as functions of k, and instead regard $\mathcal{X}_n$ and $\mathcal{Y}_n$ as polynomials of degree n in the variable $\mathcal{T}$ (recall that $\mathcal{R} = 1 - \mathcal{T}$), with f_L and f_R being some fixed parameters. Recall that n is taken to be an even integer, such that $\mathcal{Y}_n$ is indeed a polynomial in $\mathcal{T}$ even though its definition formally contains non-integer powers of $\mathcal{T}$, as these powers cancel out when summing the different terms in Eq. (55).

To prove that $\mathcal{X}_n$ and $\mathcal{Y}_n$ are identical as polynomials in $\mathcal{T}$, it suffices to show that they agree at a certain point, say $\mathcal{T} = 0$, and that they have the same n roots when $\mathcal{T}$ is seen as a complex variable. The former requirement is simpler: it is easy to check that substituting $\mathcal{T} = 0$ into both polynomials (i.e., into Eqs. (55) and (C3)) yields

$$\mathcal{X}_n(\mathcal{T} = 0) = [(f_L)^n + (1 - f_L)^n][(f_R)^n + (1 - f_R)^n]$$
$$= \mathcal{Y}_n(\mathcal{T} = 0). \tag{C4}$$

As for the latter requirement regarding the equality between the roots of the two polynomials, we may extract these roots using the fact that in Eq. (C3) $\mathcal{X}_n$ is already written as a product of terms that are linear in $\mathcal{T}$. Its n

roots are thus given by

$$\mathcal{T}_\gamma = \frac{\left[1 - \left(1 - e^{\frac{2\pi i\gamma}{n}}\right) f_L\right]\left[1 - \left(1 + e^{\frac{-2\pi i\gamma}{n}}\right) f_R\right]}{\left(e^{\frac{2\pi i\gamma}{n}} + e^{\frac{-2\pi i\gamma}{n}}\right)(f_L - f_R)}. \tag{C5}$$

For convenience, we also define $\mathcal{R}_\gamma = 1 - \mathcal{T}_\gamma$. Now we must show that $\mathcal{Y}_n(\mathcal{T}_\gamma) = 0$ for all γ. Indeed, one may check that the substitution of $\mathcal{T}_\gamma$ into the first two square-bracketed summands in Eq. (55) yields

$$[\mathcal{T}_\gamma f_L + \mathcal{R}_\gamma f_R - f_L f_R]^n + [\mathcal{R}_\gamma f_L + \mathcal{T}_\gamma f_R - f_L f_R]^n$$
$$= \left[\frac{1 - \left(1 - e^{\frac{2\pi i\gamma}{n}}\right)(f_L + f_R) - 2e^{\frac{2\pi i\gamma}{n}} f_L f_R}{e^{\frac{2\pi i\gamma}{n}} + e^{\frac{-2\pi i\gamma}{n}}}\right]^n$$
$$+ \left[\frac{1 - \left(1 + e^{\frac{-2\pi i\gamma}{n}}\right)(f_L + f_R) + 2e^{\frac{-2\pi i\gamma}{n}} f_L f_R}{e^{\frac{2\pi i\gamma}{n}} + e^{\frac{-2\pi i\gamma}{n}}}\right]^n. \tag{C6}$$

On the other hand, we observe that

$$\left[\frac{1 - f_L - f_R + 2f_L f_R}{2}\right]^2 + \mathcal{T}_\gamma \mathcal{R}_\gamma (f_L - f_R)^2$$
$$= \left[\frac{\left(e^{\frac{-2\pi i\gamma}{n}} - e^{\frac{2\pi i\gamma}{n}}\right)\frac{1 - f_L - f_R}{2} + f_L + f_R - 2f_L f_R}{e^{\frac{2\pi i\gamma}{n}} + e^{\frac{-2\pi i\gamma}{n}}}\right]^2, \tag{C7}$$

which is equivalent to the statement that

$$\sqrt{\left[\frac{1 - f_L - f_R + 2f_L f_R}{2}\right]^2 + \mathcal{T}_\gamma \mathcal{R}_\gamma (f_L - f_R)^2}$$
$$= \pm \frac{e^{\mp \frac{2\pi i\gamma}{n}}}{e^{\frac{2\pi i\gamma}{n}} + e^{\frac{-2\pi i\gamma}{n}}}\left[1 - \left(1 \mp e^{\pm\frac{2\pi i\gamma}{n}}\right)(f_L + f_R)\right.$$
$$\mp 2e^{\pm\frac{2\pi i\gamma}{n}} f_L f_R\right] \mp \frac{1 - f_L - f_R}{2}. \tag{C8}$$

Thus, using the identities in Eqs. (C6) and (C8) as well as the fact that $\left(e^{\frac{2\pi i\gamma}{n}}\right)^n = -1$ for all γ, we conclude that in fact $\mathcal{Y}_n(\mathcal{T}_\gamma) = 0$ for all γ, which completes the proof.

[1] M. Serbyn, Z. Papić, and D. A. Abanin, Local conservation laws and the structure of the many-body localized states, Phys. Rev. Lett. **111**, 127201 (2013).

[2] H. Kim and D. A. Huse, Ballistic spreading of entanglement in a diffusive nonintegrable system, Phys. Rev. Lett. **111**, 127205 (2013).

[3] R. Nandkishore and D. A. Huse, Many-body localization and thermalization in quantum statistical mechanics, Annual Review of Condensed Matter Physics **6**, 15 (2015).

[4] L. D'Alessio, Y. Kafri, A. Polkovnikov, and M. Rigol, From quantum chaos and eigenstate thermalization to statistical mechanics and thermodynamics, Advances in Physics **65**, 239 (2016).

[5] V. Alba and P. Calabrese, Entanglement and thermodynamics after a quantum quench in integrable systems, Proceedings of the National Academy of Sciences **114**, 7947 (2017).

[6] J. M. Deutsch, Eigenstate thermalization hypothesis, Reports on Progress in Physics **81**, 082001 (2018).

[7] V. Alba and P. Calabrese, Entanglement dynamics after quantum quenches in generic integrable systems, SciPost Phys. **4**, 17 (2018).

[8] D. A. Abanin, E. Altman, I. Bloch, and M. Serbyn, Colloquium: Many-body localization, thermalization, and entanglement, Rev. Mod. Phys. **91**, 021001 (2019).

[9] M. Serbyn, D. A. Abanin, and Z. Papić, Quantum many-body scars and weak breaking of ergodicity, Nature Physics **17**, 675 (2021).

[10] M. Mestyán, B. Bertini, L. Piroli, and P. Calabrese, Exact solution for the quench dynamics of a nested integrable system, Journal of Statistical Mechanics: Theory and Experiment **2017**, 083103 (2017).

[11] V. Alba and P. Calabrese, Quantum information dynamics in multipartite integrable systems, EPL (Europhysics Letters) **126**, 60001 (2019).

[12] V. Alba and P. Calabrese, Quantum information scrambling after a quantum quench, Phys. Rev. B **100**, 115150 (2019).

[13] P. Hayden and J. Preskill, Black holes as mirrors: quantum information in random subsystems, Journal of High Energy Physics **2007**, 120 (2007).

[14] B. Swingle, Unscrambling the physics of out-of-time-order correlators, Nature Physics **14**, 988 (2018).

[15] S. Xu and B. Swingle, Scrambling dynamics and out-of-time-ordered correlators in quantum many-body systems, PRX Quantum **5**, 010201 (2024).

[16] M. J. Gullans and D. A. Huse, Entanglement structure of current-driven diffusive fermion systems, Phys. Rev. X **9**, 021007 (2019).

[17] M. J. Gullans and D. A. Huse, Localization as an entanglement phase transition in boundary-driven Anderson models, Phys. Rev. Lett. **123**, 110601 (2019).

[18] L. Hruza and D. Bernard, Coherent fluctuations in noisy mesoscopic systems, the open quantum SSEP, and free probability, Phys. Rev. X **13**, 011045 (2023).

[19] S. Fraenkel and M. Goldstein, Extensive long-range entanglement in a nonequilibrium steady state, SciPost Phys. **15**, 134 (2023).

[20] D. Bernard and L. Hruza, Exact entanglement in the driven quantum symmetric simple exclusion process, SciPost Phys. **15**, 175 (2023).

[21] M. M. Wolf, F. Verstraete, M. B. Hastings, and J. I. Cirac, Area laws in quantum systems: Mutual information and correlations, Phys. Rev. Lett. **100**, 070502 (2008).

[22] M. M. Wolf, Violation of the entropic area law for fermions, Phys. Rev. Lett. **96**, 010404 (2006).

[23] D. Gioev and I. Klich, Entanglement entropy of fermions in any dimension and the Widom conjecture, Phys. Rev. Lett. **96**, 100503 (2006).

[24] P. Calabrese, J. Cardy, and E. Tonni, Entanglement entropy of two disjoint intervals in conformal field theory, Journal of Statistical Mechanics: Theory and Experiment **2009**, P11001 (2009).

[25] V. Eisler and Z. Zimborás, Area-law violation for the mutual information in a nonequilibrium steady state, Phys. Rev. A **89**, 032321 (2014).

[26] V. Eisler, Entanglement negativity in a nonequilibrium steady state, Phys. Rev. B **107**, 075157 (2023).

[27] V. Eisler and I. Peschel, On entanglement evolution across defects in critical chains, EPL (Europhysics Letters) **99**, 20001 (2012).

[28] H. Saleur, P. Schmitteckert, and R. Vasseur, Entanglement in quantum impurity problems is nonperturbative, Phys. Rev. B **88**, 085413 (2013).

[29] M. Ljubotina, S. Sotiriadis, and T. Prosen, Non-equilibrium quantum transport in presence of a defect: the non-interacting case, SciPost Phys. **6**, 004 (2019).

[30] M. Gruber and V. Eisler, Time evolution of entanglement negativity across a defect, Journal of Physics A: Mathematical and Theoretical **53**, 205301 (2020).

[31] V. Alba, Unbounded entanglement production via a dissipative impurity, SciPost Phys. **12**, 11 (2022).

[32] A. Roy and H. Saleur, Entanglement entropy in the Ising model with topological defects, Phys. Rev. Lett. **128**, 090603 (2022).

[33] L. Capizzi, S. Scopa, F. Rottoli, and P. Calabrese, Domain wall melting across a defect, Europhysics Letters **141**, 31002 (2023).

[34] D. X. Horváth, S. Fraenkel, S. Scopa, and C. Rylands, Charge-resolved entanglement in the presence of topological defects, Phys. Rev. B **108**, 165406 (2023).

[35] L. Capizzi, S. Murciano, and P. Calabrese, Full counting statistics and symmetry resolved entanglement for free conformal theories with interface defects, Journal of Statistical Mechanics: Theory and Experiment **2023**, 073102 (2023).

[36] G. Gouraud, P. Le Doussal, and G. Schehr, Stationary time correlations for fermions after a quench in the presence of an impurity, Europhysics Letters **142**, 41001 (2023).

[37] L. Capizzi and V. Eisler, Entanglement evolution after a global quench across a conformal defect, SciPost Phys. **14**, 070 (2023).

[38] C. Rylands and P. Calabrese, Transport and entanglement across integrable impurities from generalized hydrodynamics, Phys. Rev. Lett. **131**, 156303 (2023).

[39] D. A. Abanin and E. Demler, Measuring entanglement entropy of a generic many-body system with a quantum switch, Phys. Rev. Lett. **109**, 020504 (2012).

[40] A. J. Daley, H. Pichler, J. Schachenmayer, and P. Zoller, Measuring entanglement growth in quench dynamics of

bosons in an optical lattice, Phys. Rev. Lett. **109**, 020505 (2012).

[41] R. Islam, R. Ma, P. M. Preiss, M. Eric Tai, A. Lukin, M. Rispoli, and M. Greiner, Measuring entanglement entropy in a quantum many-body system, Nature **528**, 77 (2015).

[42] A. Elben, B. Vermersch, M. Dalmonte, J. I. Cirac, and P. Zoller, Rényi entropies from random quenches in atomic Hubbard and spin models, Phys. Rev. Lett. **120**, 050406 (2018).

[43] E. Cornfeld, E. Sela, and M. Goldstein, Measuring fermionic entanglement: Entropy, negativity, and spin structure, Phys. Rev. A **99**, 062309 (2019).

[44] R. Horodecki, P. Horodecki, M. Horodecki, and K. Horodecki, Quantum entanglement, Rev. Mod. Phys. **81**, 865 (2009).

[45] B. Groisman, S. Popescu, and A. Winter, Quantum, classical, and total amount of correlations in a quantum state, Phys. Rev. A **72**, 032317 (2005).

[46] M. Kormos and Z. Zimborás, Temperature driven quenches in the Ising model: appearance of negative Rényi mutual information, Journal of Physics A: Mathematical and Theoretical **50**, 264005 (2017).

[47] S. O. Scalet, Á. M. Alhambra, G. Styliaris, and J. I. Cirac, Computable Rényi mutual information: Area laws and correlations, Quantum **5**, 541 (2021).

[48] J. Kudler-Flam, Rényi mutual information in quantum field theory, Phys. Rev. Lett. **130**, 021603 (2023).

[49] H. Shapourian, K. Shiozaki, and S. Ryu, Partial time-reversal transformation and entanglement negativity in fermionic systems, Phys. Rev. B **95**, 165101 (2017).

[50] G. Vidal and R. F. Werner, Computable measure of entanglement, Phys. Rev. A **65**, 032314 (2002).

[51] M. B. Plenio, Logarithmic negativity: A full entanglement monotone that is not convex, Phys. Rev. Lett. **95**, 090503 (2005).

[52] J. Eisert, V. Eisler, and Z. Zimborás, Entanglement negativity bounds for fermionic Gaussian states, Phys. Rev. B **97**, 165123 (2018).

[53] H. Shapourian and S. Ryu, Finite-temperature entanglement negativity of free fermions, Journal of Statistical Mechanics: Theory and Experiment **2019**, 043106 (2019).

[54] P. Ruggiero, V. Alba, and P. Calabrese, Negativity spectrum of one-dimensional conformal field theories, Phys. Rev. B **94**, 195121 (2016).

[55] H. Shapourian, P. Ruggiero, S. Ryu, and P. Calabrese, Twisted and untwisted negativity spectrum of free fermions, SciPost Phys. **7**, 037 (2019).

[56] R. G. Newton, Inverse scattering by a local impurity in a periodic potential in one dimension, Journal of Mathematical Physics **24**, 2152 (1983).

[57] E. Merzbacher, *Quantum Mechanics* (Wiley, 1998) pp. 80–115.

[58] B. Bertini, K. Klobas, and T.-C. Lu, Entanglement negativity and mutual information after a quantum quench: Exact link from space-time duality, Phys. Rev. Lett. **129**, 140503 (2022).

[59] H. Shapourian and S. Ryu, Entanglement negativity of fermions: Monotonicity, separability criterion, and classification of few-mode states, Phys. Rev. A **99**, 022310 (2019).

[60] V. Alba and F. Carollo, Logarithmic negativity in out-of-

equilibrium open free-fermion chains: An exactly solvable case, SciPost Phys. **15**, 124 (2023).

[61] F. Caceffo and V. Alba, Entanglement negativity in a fermionic chain with dissipative defects: exact results, Journal of Statistical Mechanics: Theory and Experiment **2023**, 023102 (2023).

[62] F. Ares, S. Murciano, E. Vernier, and P. Calabrese, Lack of symmetry restoration after a quantum quench: An entanglement asymmetry study, SciPost Phys. **15**, 089 (2023).

[63] I. Peschel, Calculation of reduced density matrices from correlation functions, Journal of Physics A: Mathematical and General **36**, L205 (2003).

[64] R. Wong, *Asymptotic Approximations of Integrals* (SIAM, 2001) pp. 477–515.

[65] H. Widom, Asymptotic behavior of block Toeplitz matrices and determinants, Advances in Mathematics **13**, 284 (1974).

[66] X. Turkeshi, L. Piroli, and M. Schiró, Enhanced entanglement negativity in boundary-driven monitored fermionic chains, Phys. Rev. B **106**, 024304 (2022).

[67] I. Klich and L. Levitov, Many-body entanglement: a new application of the full counting statistics, AIP Conference Proceedings **1134**, 36 (2009).

[68] O. Gamayun, O. Lychkovskiy, and J.-S. Caux, Fredholm determinants, full counting statistics and Loschmidt echo for domain wall profiles in one-dimensional free fermionic chains, SciPost Phys. **8**, 36 (2020).

[69] B. Bertini, P. Calabrese, M. Collura, K. Klobas, and C. Rylands, Nonequilibrium full counting statistics and symmetry-resolved entanglement from space-time duality, Phys. Rev. Lett. **131**, 140401 (2023).

[70] M. Goldstein and E. Sela, Symmetry-resolved entanglement in many-body systems, Phys. Rev. Lett. **120**, 200602 (2018).

[71] E. Cornfeld, M. Goldstein, and E. Sela, Imbalance entanglement: Symmetry decomposition of negativity, Phys. Rev. A **98**, 032302 (2018).

[72] N. Feldman and M. Goldstein, Dynamics of charge-resolved entanglement after a local quench, Phys. Rev. B **100**, 235146 (2019).

[73] R. Bonsignori, P. Ruggiero, and P. Calabrese, Symmetry resolved entanglement in free fermionic systems, Journal of Physics A: Mathematical and Theoretical **52**, 475302 (2019).

[74] S. Fraenkel and M. Goldstein, Symmetry resolved entanglement: exact results in 1D and beyond, Journal of Statistical Mechanics: Theory and Experiment **2020**, 033106 (2020).

[75] S. Murciano, R. Bonsignori, and P. Calabrese, Symmetry decomposition of negativity of massless free fermions, SciPost Phys. **10**, 111 (2021).

[76] G. Parez, R. Bonsignori, and P. Calabrese, Exact quench dynamics of symmetry resolved entanglement in a free fermion chain, Journal of Statistical Mechanics: Theory and Experiment **2021**, 093102 (2021).

[77] S. Zhao, C. Northe, and R. Meyer, Symmetry-resolved entanglement in AdS_3/CFT_2 coupled to $U(1)$ Chern-Simons theory, Journal of High Energy Physics **2021**, 30 (2021).

[78] P. Calabrese and J. Cardy, Entanglement entropy and quantum field theory, Journal of Statistical Mechanics: Theory and Experiment **2004**, P06002 (2004).

[79] A. Kitaev and J. Preskill, Topological entanglement en-

tropy, Phys. Rev. Lett. **96**, 110404 (2006).

[80] S. Fraenkel and M. Goldstein, Exact asymptotics of long-range quantum correlations in a non-equilibrium steady state, Journal of Statistical Mechanics: Theory and Experiment **2024**, 033107 (2024).

[81] P. Calabrese and J. Cardy, Entanglement entropy and conformal field theory, Journal of Physics A: Mathematical and Theoretical **42**, 504005 (2009).

[82] P. Calabrese and J. Cardy, Evolution of entanglement entropy in one-dimensional systems, Journal of Statistical Mechanics: Theory and Experiment **2005**, P04010 (2005).

[83] B. Bertini, K. Klobas, V. Alba, G. Lagnese, and P. Calabrese, Growth of Rényi entropies in interacting integrable models and the breakdown of the quasiparticle picture, Phys. Rev. X **12**, 031016 (2022).

[84] F. Carollo and V. Alba, Entangled multiplets and spreading of quantum correlations in a continuously monitored tight-binding chain, Phys. Rev. B **106**, L220304 (2022).

[85] M. Brenes, E. Mascarenhas, M. Rigol, and J. Goold, High-temperature coherent transport in the XXZ chain in the presence of an impurity, Phys. Rev. B **98**, 235128 (2018).

[86] A. Bastianello, Lack of thermalization for integrability-breaking impurities, Europhysics Letters **125**, 20001

(2019).

[87] M. Brenes, T. LeBlond, J. Goold, and M. Rigol, Eigenstate thermalization in a locally perturbed integrable system, Phys. Rev. Lett. **125**, 070605 (2020).

[88] A.-M. Visuri, T. Giamarchi, and C. Kollath, Symmetry-protected transport through a lattice with a local particle loss, Phys. Rev. Lett. **129**, 056802 (2022).

[89] M. Žnidarič, Entanglement in stationary nonequilibrium states at high energies, Phys. Rev. A **85**, 012324 (2012).

[90] J. Erdmenger, D. Fernández, M. Flory, E. Megías, A.-K. Straub, and P. Witkowski, Time evolution of entanglement for holographic steady state formation, Journal of High Energy Physics **2017**, 34 (2017).

[91] C. Ecker, J. Erdmenger, and W. van der Schee, Non-equilibrium steady state formation in 3+1 dimensions, SciPost Phys. **11**, 047 (2021).

[92] A. M. Kaufman, M. E. Tai, A. Lukin, M. Rispoli, R. Schittko, P. M. Preiss, and M. Greiner, Quantum thermalization through entanglement in an isolated many-body system, Science **353**, 794 (2016).

[93] M. Tajik, I. Kukuljan, S. Sotiriadis, B. Rauer, T. Schweigler, F. Cataldini, J. Sabino, F. Møller, P. Schüttelkopf, S.-C. Ji, D. Sels, E. Demler, and J. Schmiedmayer, Verification of the area law of mutual information in a quantum field simulator, Nature Physics **19**, 1022 (2023).